PERGAMON

Chaos, Solitons and Fractals 11 (2000) 961–985

CHAOS
SOLITONS & FRACTALS

www.elsevier.nl/locate/chaos

Global dynamics in a non-linear model of the equity ratio

Anna Agliari [a], Laura Gardini [a,b,*], Domenico Delli Gatti [c], Mauro Gallegati [d]

[a] *University di Parma, Faculty of Economics, Viale Kennedy, Italy*
[b] *Instituto di Scienze Economiche, University di Parma and University of Urbino, 61029 Urbino, Italy*
[c] *Catholic University in Milan, Italy*
[d] *University of Teramo, Italy*

Accepted 5 October 1998

Abstract

A model for firms' financial conditions is proposed, which ultimately reduces to a two-dimensional non-invertible map in the variables mean and variance of the equity ratio. The possible dynamics of the model and the global behaviour are investigated. We describe the mechanism of bifurcations leading to fractalization of the basins and/or fractalization of their boundaries, showing how a *locally stable* attractor may be *almost globally unstable*. Multistability is also investigated. Two, three or four co-existing attractors have been found and we describe the mechanism of bifurcations leading their basins to become chaotically intermingled, and thus to unpredictability of the asymptotic state in a wide region. The knowledge of such regimes, besides those associated with simple dynamics, may be of help for the operators. While the use of the technical tools we propose to study the global dynamics and bifurcations may be of help for further investigations. © 2000 Elsevier Science Ltd. All rights reserved.

1. Introduction

In this paper we present a model of fluctuating growth in which firms' financial conditions play a crucial role. Our analysis starts from the distribution of firms according to their *equity ratio*, that is the ratio of the equity base or net worth to the capital stock, a proxy of financial robustness. We identify two dynamic laws for the mean and the variance of this distribution. The motion over time of the average equity ratio is the engine of growth and fluctuations. The dynamic pattern of the dispersion of the distribution, captured by the variance, however, interacts with evolution of the average equity ratio.

Given the non-linear nature of the map which describes the laws of motion of the mean and the variance of the equity ratio, a wide range of dynamic patterns are possible. Fixed points or periodic orbits, attracting closed invariant curves and thin annular chaotic areas wide chaotic areas or explosions may occur. For quite plausible values of the parameters which characterize the map, the dynamics of the equity ratio can be regular or chaotic, and the motion of capital and output can be characterized as a process of fluctuating growth, although, as we shall see, often very sensitive to small perturbations.

The goal of the present paper is to show how the global properties (deriving from the structure of the basins, their boundaries and the critical curves of non-invertible two-dimensional maps) may be used to understand the dynamic behaviour of the model, especially when analytical results are not accessible, as in our case, where not only the equilibrium values, but also the number of existing fixed points, cannot be explicitly known.

* Corresponding author. Fax: +39-722-327-655.
E-mail addresses: agliari@ipruniv.cce.unipr.it (A. Agliari), gardini@econ.uniurb.it (L. Gardini), delliga@mi.unicatt.it (D.D. Gatti), gallegati@deanovell.unian.it (M. Gallegati).

0960-0779/00/$ - see front matter
PII: S0960-0779(98)00258-6

The paper is organized as follows. In Section 2 we briefly describe the general features of the economy under scrutiny. Moreover, we derive the optimal ratio of the output supplied to the capital stock and the investment ratio. In Section 3 we describe the model governing the dynamics of the average equity ratio and of the variance, whose generic properties are given in Section 4. It is shown that analytical results cannot be obtained in general. However, the model can be considered as a perturbation of the symmetric distribution case, also of interest. This is simpler to investigate by qualitative and analytical methods, as described in Section 5, where the main results are presented. In Section 5.1 we show how the global dynamics are important in order to classify a locally stable attractor as suitable for the applications or not, depending on the shape and structure of its basin of attraction. Several kinds of global bifurcations are evidenced, which involve the frontiers of the basins of attraction and their contacts with the critical curves of the non-invertible map, as described in [1,2]. The different situations shown in this paper constitute an exemplary "route" of sequences of bifurcations, of fundamental importance (both in a theoretical and applicative framework). We hope to contribute, with this paper, to the divulgation of such kinds of bifurcation mechanisms and of the technical tools to detect them.

Another peculiarity of the model is the co-existence of several different attractors. As shown in Section 5.2, the global properties show that although only simple attractors exist (as fixed points or cycles of low period), we may have unpredictability of the asymptotic behaviour, due to the existence of chaotically intermingled basins. The results of Section 5 are used to understand the dynamics of the more generic model, described in Section 6. Some conclusions are drawn in Section 7.

2. The behaviour of firms

We consider a closed economy populated by firms, households and banks. Households demand consumption goods and supply labour services. Banks extend credit to firms at a given interest rate. We do not dig deeper into the microfoundations of households and banks' behaviour (on this issue see [3]) and focus on firms instead.

There is a large number of price-taking firms which produce a homogeneous good by means of capital and labour and accumulate capital (invest) in order to expand productive capacity when the actual capital stock is smaller than the target ("desired") level. Firms are heterogeneous with respect to their financial robustness captured by the equity ratio, i.e. the ratio of the equity base or net worth to the capital stock. In other words the equity ratio of the ith firm at time t, say a_{it} is a random variable with mean $E(a_{it}) = a_t$ and variance $E(a_{it} - a_t)^2 = V_t$.

The ith firm carries on production (Y_i) by means of a "well behaved" production function which uses capital (K_i) and labour (N_i) as inputs : $Y_i = F(\upsilon N_i, K_i)$. υ is a technological shock uniform across firms and $F(\cdot)$ is homogeneous of degree one. Thanks to the homogeneity assumption, the production function can be written in intensive form as follows

$$y_i = f(\upsilon n_i), \tag{1}$$

where $y_i = Y_i/K_i,\ n_i = N_i/K_i,\ f_n > 0,\ f_{nn} < 0$.

Therefore, the labour requirement function is

$$n_i = \frac{\varphi(y_i)}{\upsilon}, \tag{2}$$

where $\varphi_y > 0,\ \varphi_{yy} > 0$.

Each firm is not sure at which price it will sell its goods. The relative price, i.e. the ratio of the individual selling price to the average price level $u_i = P_i/P$ is a random variable with distribution function $\Psi(\cdot)$, expected value $u^e = P^e/P$ and finite variance σ_u^2. For the sake of simplicity, we assume that the expected relative price is the same for each and every firm (homogeneous expectations).

Therefore profit in real terms will be

$$\Pi_i = u_i Y_i - r(wN_i + K_i),$$

where r and w are the (gross) interest rate charged by the banks and the real wage respectively, which will be given and uniform across firms.

Firms cannot raise external finance on the equity market (see [4]) so that they have to rely on credit in order to finance production. Therefore, they run the risk of bankruptcy. The firm goes bankrupt if the real profit becomes negative. This bankruptcy condition occurs if the actual selling price, i.e. the realization of the random relative price u_i, happens to be lower than the average cost $\bar{u}_i$, which in turn is equal to debt per unit of output. The probability of bankruptcy therefore is: $\Pr(u_i < \bar{u}_i) = \Psi(\bar{u}_i)$, $\Psi_u > 0$, where

$$\bar{u}_i = r\frac{wN_i + K_i}{Y_i}.$$

We assume that the distribution of the relative price is uniform, with support $[0, \hat{u}]$. The probability of bankruptcy therefore is

$$\Pr\left(u_i < \bar{u}_i\right) = \frac{\bar{u}_i}{\hat{u}} = r\frac{wN_i + K_i}{\hat{u}Y_i}.$$

Bankruptcy is costly and the cost of bankruptcy is increasing with the scale of production and decreasing with the equity ratio: $CB_i = c(a_{it-1})Y_i$, $c_a < 0$. On bankruptcy costs see [5–8].

2.1. Supply

Since capital is a fixed factor of production in the short run, we can formulate the problem of the firm in intensive form as follows:

$$\underset{y_i}{\mathrm{Max}} E(\pi_i) - CB_i \Pr\left(u_i < \bar{u}_i\right) = u^e y_i - R(r, a_{it-1})\left[\frac{w}{\upsilon}\varphi(y_i) + 1\right], \tag{3}$$

where π_i is the profit rate, $\varphi(y_i)/\upsilon$ is the labour requirement function (see (2)) and

$$R(r, a_{it-1}) = r\left[1 + \frac{c(a_{it-1})}{\hat{u}}\right]$$

is the *bankruptcy cost augmented interest rate*, i.e. the interest rate as perceived by the firm, which includes the borrower's risk [9,10].

From the first order condition of (3) we obtain

$$y_i = \varphi_y^{-1}\left(\frac{\upsilon u^e}{R(r, a_{it-1})w}\right). \tag{4}$$

For the sake of simplicity we will assume that (4) is linear in a_{it-1} so that it can be rewritten as follows:

$$y_i = \phi(r, w, \upsilon, u^e)a_{it-1}. \tag{5}$$

Let y and a_{t-1} be the average supply and the average equity ratio, respectively. Thanks to the linearity assumption above, we can write the average supply as

$$y = \phi(r, w, \upsilon, u^e)a_{t-1}. \tag{6}$$

2.2. Investment

Capital is a fixed factor of production in the short run. In the long run, however, it becomes variable. Long run profit maximization requires the equality of the technical rate of substitution and the relative price of inputs

$$\frac{F_N(\upsilon N_i, K_i)}{F_K(\upsilon N_i, K_i)} = \frac{R(r, a_{it-1})w}{R(r, a_{it-1})} = w.$$

From the equation above we can derive the long run (optimal) capital-labour ratio, which in turn will depend only on the technological parameter and the real wage. The long run capital output ratio (say k) is a monotonic increasing transformation of the capital-labour ratio. It too, therefore, will depend only on the technological parameter and the real wage.

For each firm, investment is proportional to the difference between the long run optimal or desired capital stock (kY_i) and the stock of capital inherited from the past (K_{it-1}):

$$I_i = \lambda(kY_i - K_{it-1}), \tag{7}$$

where λ is the stock adjustment parameter, $(0 < \lambda < 1)$.

Taking into account (7) and assuming that there is no capital depreciation, the law of motion of the capital stock can be written as follows: $K_i = K_{it-1} + I_i = K_{it-1}(1-\lambda) + \lambda k Y_i$. Dividing by the stock of capital and rearranging we get

$$\frac{K_{it-1}}{K_i} = \frac{1-\lambda k y_i}{1-\lambda}. \tag{8}$$

3. The dynamic model

The level of net worth in real terms for the ith firm is

$$A_{it} = A_{it-1} + u^e Y_i - r(wN_i + K_i).$$

Dividing by the capital stock we obtain the law of motion of the equity ratio

$$a_{it} = a_{it-1}\frac{K_{it-1}}{K_i} + u^e y_i - r(wn_i + 1).$$

Recalling (8) and (5) from the expression above we obtain

$$a_{it} = a_{it-1}\frac{1-\lambda k\phi(r,w,\upsilon,u^e)a_{it-1}}{1-\lambda} + u^e\phi(r,w,\upsilon,u^e)a_{it-1} - r[w\varphi(\phi(r,w,\upsilon,u^e)a_{it-1}) + 1]. \tag{9}$$

The model we study in the following is obtained by specifying the production function in (1) as the Cobb–Douglas function:

$$Y_i = (\upsilon N_i)^{\zeta} K_i^{1-\zeta} \quad 0 < \zeta < 1$$

and the function $R(\cdot)$ in (3)) as

$$R(r, a_{it-1}) = \frac{r}{a_{it-1}}.$$

Thus (4) becomes

$$y_i = \left(\frac{\upsilon u^e \zeta}{rw} a_{it-1}\right)^{\zeta/(1-\zeta)}. \tag{10}$$

Assuming $\zeta = 1/2$, (10) becomes linear in a_{it-1}:

$$y_i = \frac{\upsilon u^e}{2rw} a_{it-1}. \tag{11}$$

Thanks to the linearity assumption above, we can write the average supply (11) as

$$y = \frac{\upsilon u^e}{2rw} a_{t-1}. \tag{12}$$

Under these assumptions, the desired capital-output ratio turns out to be

$$k = \left(\frac{w}{\upsilon}\right)^{1/2}. \tag{13}$$

Now, using the expression for $\phi(\cdot)$ deduced from (12), (9) becomes

$$a_{it} = a_{it-1}\frac{1-\lambda k(\upsilon u^e/2rw)a_{it-1}}{1-\lambda} + \frac{\upsilon(u^e)^2}{2rw}a_{it-1} - r\left[\frac{w}{\upsilon}\left(\frac{\upsilon u^e}{2rw}a_{it-1}\right)^2 + 1\right].$$

After some tidying up we obtain

$$a_{it} = -\Gamma_0 + \Gamma'_1 a_{it-1} - \Gamma'_2 a^2_{it-1}, \tag{14}$$

where

$$\Gamma_0 = r, \Gamma'_1 = \frac{1}{(1-\lambda)} + \frac{\upsilon(u^e)^2}{2rw} \quad \text{and} \quad \Gamma'_2 = \left(\frac{\lambda k}{1-\lambda} + \frac{u^e}{2}\right)\frac{\upsilon u^e}{2rw}.$$

Averaging across firms, substituting k given in (13), and assuming $u^e = 1$, from (14) we obtain the law of motion of the average equity ratio

$$a_t = -\Gamma_0 + \Gamma_1 a_{t-1} - \Gamma_2 a^2_{t-1} - \Gamma_2 V_{t-1}, \tag{15}$$

where

$$\Gamma_0 = r, \quad \Gamma_1 = \frac{1}{1-\lambda} + \frac{\upsilon}{2rw}, \quad \Gamma_2 = \frac{\lambda}{2r(1-\lambda)}\left(\frac{\upsilon}{w}\right)^{1/2} + \frac{\upsilon}{4rw}. \tag{16}$$

Consider now the variance of the equity ratio

$$V_t = E\Big(-\Gamma_0 + \Gamma'_1 a_{it-1} - \Gamma'_2 a^2_{it-1} - a_t\Big)^2.$$

After some tedious calculations we get

$$V_t = \Gamma_2^2(\beta-1)V^2_{t-1} + (2\Gamma_2 a - \Gamma_1)^2 V_{t-1} + 4\Gamma_2^2\Gamma_3 a_t - 2\Gamma_1\Gamma_2\Gamma_3, \tag{17}$$

where Γ_3 is the third moment from the mean and β is the coefficient which measures the degree of kurtosis of the distribution of the equity ratio. We shall assume that Γ_3 and β are exogenous constants.

The study of the dynamical properties of the model (15) and (17) allows to explore on the long-run behaviour of the distribution of the equity ratio, as captured by its mean and variance, starting from a given initial condition.

4. Some general properties

As described in Section 3, the time evolution of the mean and the variance of the equity ratio is obtained by the iteration of a two-dimensional map $T : (a, V) \to (a', V')$ given by

$$T : \begin{cases} a' = -\Gamma_0 + \Gamma_1 a - \Gamma_2 a^2 - \Gamma_2 V, \\ V' = \Gamma_2^2(\beta-1)V^2 + (2\Gamma_2 a - \Gamma_1)^2 V + 4\Gamma_2^2\Gamma_3 a - 2\Gamma_1\Gamma_2\Gamma_3, \end{cases} \tag{18}$$

where the coefficients

$$\Gamma_0 = r > 0, \qquad \Gamma_1 = \frac{1}{1-\lambda} + \frac{v}{2rw} > 0, \qquad \Gamma_2 = \frac{\lambda}{2r(1-\lambda)}\sqrt{\frac{\upsilon}{w}} + \frac{\upsilon}{4rw} > 0, \tag{19}$$

depend on the relevant parameters: the interest rate r, the ratio υ/w (between a technological shock υ and the real wage rate w), and the stock adjustment parameter λ $(0 < \lambda < 1)$.

In (18) the symbol $'$ denotes the unit time advancement operator, that is, if the right-hand side variables are mean and variance at time $(t-1)$ then the left-hand ones represent mean and variance at time t.

The study of the attracting sets of the map T and of their basins of attraction is not an easy task. The map (18) is a non-invertible map of the plane, that is, starting from some initial values for mean and variance, say (a_0, V_0), the iteration of (18) uniquely defines the trajectory $(a(t), V(t)) = T^t(a_0, V_0)$,

$t = 1, 2, \ldots$, whereas the backward iteration of (18) is not uniquely defined. In fact, a point (a', V') of the plane may have several pre-images, obtained by solving the algebraic system (18) with respect to a and V. Substituting the expression of V obtained from the first equation of (18) in the second one, we have an equation of 4th degree in the variable a, which can have four, two or zero solutions. Thus, following the notation used in [1,2], we expect this map to be of the so called type $Z_0 - Z_2 - Z_4$, which means that the phase plane is subdivided in different regions Z_j ($j = 0, 2, 4$) each point of which has j distinct rank-1 pre-images. Z_0 denotes a region whose points have no pre-image. Following the critical curves theory developed by Gumowski and Mira [11] and in the references given above, we look for the critical curves of rank-1 of the map, denoted by LC, which generally bound such Z_j regions. The critical curve of rank-1 is the locus of points having at least two merging rank-1 pre-images, and the locus of such *merging* rank-1 pre-images constitutes the critical curve of rank-0 of T, denoted by LC_{-1}. The images of the critical curve LC are called critical curves of higher rank: $LC_k = T^k(LC)$ for $k > 0$. This notion is the two-dimensional analogue of the notion of critical point C_{-1} of a one-dimensional map (C_{-1} local maximum or minimum), and its images, which are critical points of higher rank.

In our map (18), the critical curve LC_{-1} is given by the locus of points of the phase plane (a, V) in which the Jacobian matrix of T, say $J(a, V)$, vanishes

$$(LC_{-1}) : \mathrm{Det}\, J(a, V) = 0.$$

The critical curve LC, which separates the regions Z_0, Z_2 and Z_4, is given by the image of LC_{-1} under T

$$LC = T(LC_{-1}).$$

As we shall see, the critical curve LC_{-1} (and thus LC) is made up of two branches, say $LC_{-1} = LC_{-1}^{(a)} \cup LC_{-1}^{(b)}$, and we have $LC = LC^{(a)} \cup LC^{(b)}$. The role played by such curves is fundamental in order to understand the global bifurcations occurring both in the attracting sets and in their basins of attraction. We recall that an *attractor* A is a closed invariant set including a dense orbit, for which a neighbourhood U_1 exists such that $A \subset U_2 \subset U_1$ for a suitable neighbourhood U_2 whose points have the trajectory included in U_1 and the ω-limit set belonging to A. The *basin of attraction* of A is the set of points whose ω-limit set belongs to A. A weaker notion is that of *attracting set* (for example an attracting area), by which we mean a subset of the plane which is mapped into itself which attracts the points in a suitable neighbourhood. Moreover, in non-invertible maps we also use the notion of *absorbing areas* to denote attracting areas for which the boundary is made up of segments of critical curves. We shall see some examples in the following sections. We note that also this notion has a one-dimensional analogue in non-invertible maps, given by absorbing intervals, bounded by the images of critical points [12,1,13].

Now let us turn to the dynamics of our map T. The first problem refers to the existence of fixed points and their local stability analysis. However, this simple problem is already of not easy solution. In fact, the equilibrium points of the model are the solutions of the algebraic system

$$\begin{aligned} &-\Gamma_0 + (\Gamma_1 - 1)a - \Gamma_2 a^2 - \Gamma_2 V = 0, \\ &\Gamma_2^2(\beta - 1)V^2 + \Big((2\Gamma_2 a - \Gamma_1)^2 - 1\Big)V + 4\Gamma_2^2\Gamma_3 a - 2\Gamma_1\Gamma_2\Gamma_3 = 0, \end{aligned} \tag{20}$$

obtained by setting $a' = a$ and $V' = V$ in (18).

We can see that the system (20) has at most four real solutions. Substituting the expression of V obtained from the first equation in the second one, we get an equation of 4th degree in the variable a. In order to overcome the algebraic difficulties due to factorization of the fourth order polynomial we shall consider first the particular case occurring under the assumption $\Gamma_3 = 0$. In this case we can find the explicit solutions of the system (20), and thus of the fixed points of the map, which we shall denote by T_0. This case is not only interesting from a dynamical point of view, as we shall see in the next sections, but it also has a particular meaning from an applicative point of view. In fact, this choice corresponds to the hypothesis of symmetric distribution of the equity ratio. Moreover, this case is not too far from the other cases of applicative interest, because realistic estimations of the parameter Γ_3 give very small values, say $\Gamma_3 \in [0, 0.002]$. Thus after the study of some properties of the map T_0, in Section 5 we shall turn to the generic case, considering T as a "perturbation" of the map T_0.

We close this section noticing that in the numerical examples given in this work we assume fixed values for the rate between the technological shock υ and the wage rate w, such that $\upsilon/w = 1/3$. For the stock adjustment parameter λ the interval of interest is assumed to be $0.5 \leqslant \lambda \leqslant 0.7$. Thus we consider the maps T and T_0 when the interest rate r ($r > 0$) and the parameter λ are let to vary, in relation to different choices of the distribution parameters β and Γ_3.

5. Symmetric distribution case ($\Gamma_3 = 0$)

In this section we suppose that the equity ratio has a symmetric distribution around its mean value. This implies that in the map T (18) the parameter Γ_3 is equal to 0, and we get the following map

$$T_0 : \begin{cases} a' = -\Gamma_0 + \Gamma_1 a - \Gamma_2 a^2 - \Gamma_2 V, \\ V' = \Gamma_2^2(\beta - 1)V^2 + (2\Gamma_2 a - \Gamma_1)^2 V. \end{cases} \tag{21}$$

A first noticeable feature of the map (21) is that the coordinate axis $V = 0$ is trapping, that is, mapped into itself, since $V = 0$ gives $V' = 0$ in (21). This means that starting from an initial condition on the axis $V = 0$ (*representative agent*) the dynamics are confined to the same axis for each t, governed by the restriction of the map T_0 to that axis. Such a restriction is given by the following one-dimensional unimodal map f (obtained from the first equation in (21) with $V = 0$)

$$f : a' = -\Gamma_0 + \Gamma_1 a - \Gamma_2 a^2. \tag{22}$$

Looking for the fixed points of the one-dimensional map f, we can see that two fixed points exist iff the parameters are such that $\Delta > 0$, where

$$\Delta = (\Gamma_1 - 1)^2 - 4\Gamma_0\Gamma_2, \tag{23}$$

depends on the parameters of the model, given in (19), and in particular on the interest rate r and on the stock adjustment parameter λ. It is simple to verify that in the parameters' ranges we are considering Δ is positive, increasing with λ and decreasing with r.

In the case $\Delta \geqslant 0$ the map f in (22) is topologically conjugate to the standard logistic map

$$x' = \mu x(1 - x) \tag{24}$$

through the linear transformation

$$a = \frac{1 + \sqrt{\Delta}}{\Gamma_2} x + \frac{\Gamma_1 - 1 - \sqrt{\Delta}}{2\Gamma_2}$$

and the following relation among the parameters

$$\mu = 1 + \sqrt{\Delta}. \tag{25}$$

This means that the dynamics of (22) are completely known, as these can be obtained from those of the logistic map (24), cf. [14,11,12].

Of the two fixed points of f, $a_Q^* = (\Gamma_1 - 1 - \sqrt{\Delta})/2\Gamma_2$ and $a_P^* = (\Gamma_1 - 1 + \sqrt{\Delta})2\Gamma_2$, the fixed point a_Q^* is repelling for $\Delta > 0$, while a_P^* is attracting for $0 < \Delta < 4$. At $\Delta = 4$ a flip bifurcation occurs, which starts the well known Feigenbaum cascade of period doubling bifurcations leading to chaotic behaviour of (22). Such bifurcations of f are also bifurcations for the whole map T_0, which we shall consider depending on the parameters r and λ. Of course, the points $Q^* = (a_Q^*, 0)$ and $P^* = (a_P^*, 0)$ are fixed points of T_0 and their stability depends on the eigenvalues of the Jacobian matrix of T_0 at such points. As shown in Appendix A, the Jacobian matrix of T_0 evaluated in a point $(a, 0)$ of the a-axis is upper triangular with eigenvalues given by $\lambda_1 = (\Gamma_1 - 2\Gamma_2 a)$ and $\lambda_2 = (\lambda_1)^2$. It is easy to recognize that λ_1 is the derivative of the one-dimensional function f in a point a. From this it follows immediately:

Property 1 (Cycles of T_0 on the invariant line). *Let $\{a_1 \ldots, a_k\}$ be a k-cycle of the unimodal map $f, k \geqslant 1$, with eigenvalue λ, then $\mathscr{A}_k = \{(a_1, 0) \ldots, (a_k, 0)\}$ is a k-cycle of T_0 with eigenvalues $\lambda_1 = \lambda$ and $\lambda_2 = (\lambda)^2$.*

Moreover, from the particular structure of the Jacobian matrix $J(a,0)$ other properties can be deduced. For example, any bifurcation of a k-cycle of f is also a bifurcation of the two-dimensional map T_0. Moreover, it is a non-standard one, since both the eigenvalues cross the value +1 in modulus at the same time (i.e. it is always a co-dimension two bifurcation). Therefore, we can state the following:

Property 2 (Bifurcations of cycles of T_0 on the invariant line). *Any local bifurcation of a k-cycle of the unimodal map f, $k \geqslant 1$, is also a local bifurcation of the corresponding k-cycle A_k of T_0. A fold bifurcation of f^k gives rise to two k-cycles of T_0, a repelling node and an attracting node, while a flip bifurcation of a k-cycle of f changes an attracting node of T_0 into a repelling node giving rise to at least one attracting node of period $2k$ on the a-axis.*

As a consequence of the above properties, whenever a cycle is attracting for the restriction on the a-axis (22), it is an attracting node also for the two-dimensional map T_0, while a cycle repelling for the restriction (22) is a repelling node for T_0.

Thus, for $\Delta > 0$ the fixed point $Q^* = (a_Q^*, 0)$ is always a repelling node for T_0, whereas the point $P^* = (a_P^*, 0)$ from attracting node (for $0 < \Delta < 4$) becomes a repelling node at $\Delta = 4$, giving rise to a 2-cycle on the a-axis, attracting node. And so on. It is important to note that for the one-dimensional map f, a k-cycle or k-cyclic chaotic intervals, $k \geqslant 1$, always exists in the range $4 < \Delta \leqslant 9$. *However, only an attracting k-cycle of f is also an attractor for T_0, because when a chaotic interval exists for f, it is "transversally repelling" for T_0 and thus behaves as a chaotic saddle.*

One of the main consequences of the existence of the invariant line for the dynamics of T_0 is the *multistability*, that is, co-existence of disjoint attracting sets, one of which is with variance zero, and the others with positive variances. In fact, for $\Delta > 4$ another fixed point exists in the positive quadrant $V > 0$, denoted by R^* in Appendix A, which has intervals of stability and may become repelling, giving rise to other different attractors, all with positive variance. In these cases we are interested in the analysis of the corresponding basins of attraction, in order to see which are the points (initial conditions) whose trajectories eventually converge to each attracting set.

Among the attracting sets we have also to include attractors at infinity, on the Poincarè Equator. In fact the map T_0 can generate divergent trajectories. For example, divergent trajectories on the a-axis are obtained with the points $(a,0)$ having $a < a_Q^*$ and $a > a_{Q_{-1}}$, where $a_{Q_{-1}} = (\Gamma_1 + 1 + \sqrt{\Delta})/2\Gamma_2$ is the rank-1 pre-image of a_Q^* on the a-axis (i.e. $Q_{-1}^* = (a_{Q_{-1}}, 0)$ is the rank-1 pre-image of the fixed point Q^* belonging to the a-axis). All the points $(a,0)$ with $a \in (a_Q^*, a_{Q_{-1}})$ have bounded trajectories, with zero variance. But the attractor with zero variance has not only points of this interval in its basin. When an attracting k-cycle $\mathscr{A}_k$ exists on the a-axis its basin of attraction $\mathscr{B}(\mathscr{A}_k)$ is wider, and includes also points having positive variance.

In the following we shall see several co-existing bounded attractors (which may include fixed points, periodic orbits or more complex attractors) and we shall denote by $\mathscr{B}$ their basin of attraction. $\mathscr{B}(\infty)$ denotes the basin of the Poincarè Equator, locus of points having divergent trajectories.

An example is shown in Fig. 1(c). The parameters are such that Δ is just beyond 4, thus the fixed point P^* is a repelling node and a 2-cycle attracting node $\mathscr{A}_2 = \{(a_1,0),(a_2,0)\}$ exists on the a-axis. At the same time also the fixed point R^* is attracting. The white points of Fig. 1(c) belong to the basin $\mathscr{B}(R^*)$, the dark-grey points denote $\mathscr{B}(\mathscr{A}_2)$ and the light-grey points $\mathscr{B}(\infty)$.

A particular symmetry property is immediately evident from Fig. 1(c). That is, whichever is the attractor we are considering (at finite distance or at infinity), its basin of attraction is symmetric, as stated in the following:

Property 3 (Symmetry of the basins of T_0). *Let $\mathscr{B}$ be a basin of attraction of an attractor of T_0, then $\mathscr{B}$ is symmetric with respect to the vertical line of equation*:

$$a = \frac{\Gamma_1}{2\Gamma_2}. \tag{26}$$

That is, points which are symmetric with respect to (26) are mapped by T_0 in the same point. Actually this line of symmetry for the basins is a particular line for the map T_0. As we shall see below, it belongs to

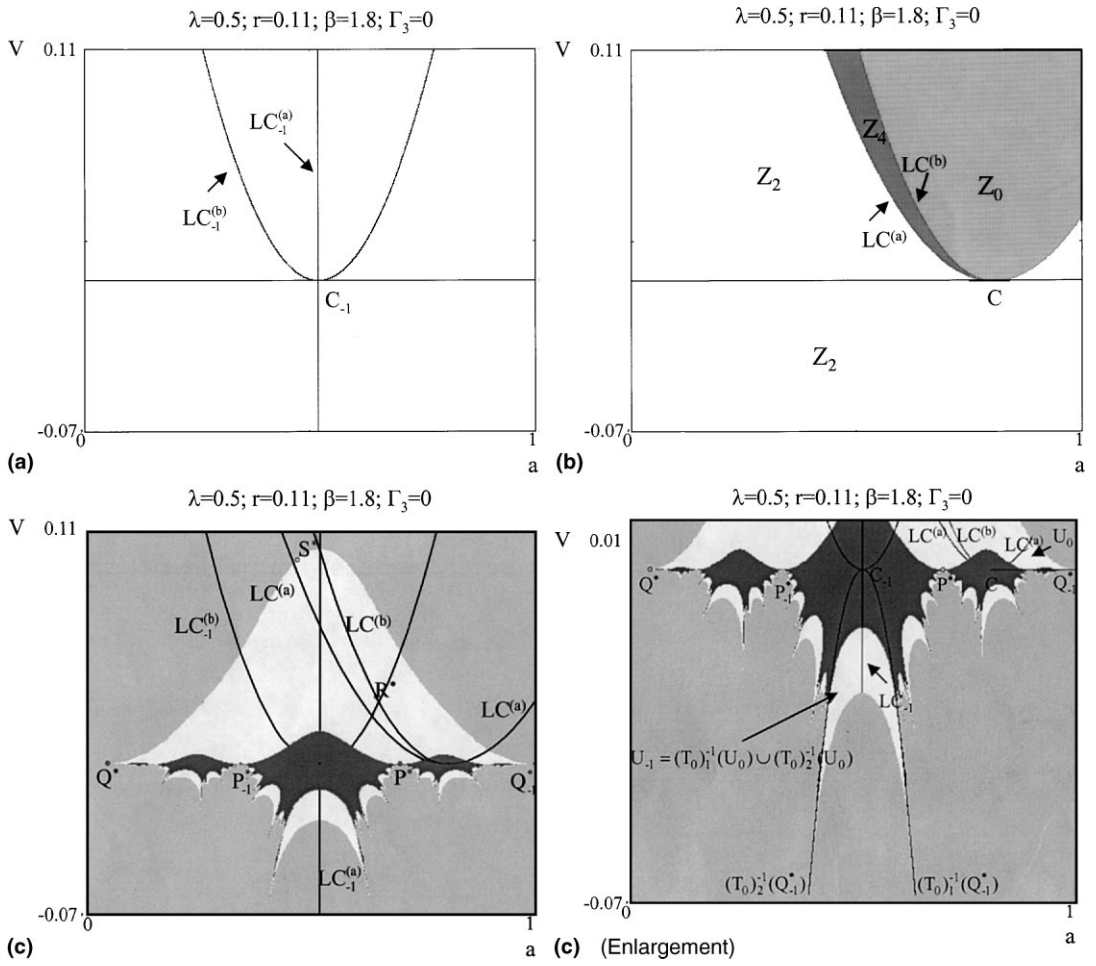

Fig. 1. (a) The critical curve LC_{-1}. The values of the parametrs are given in the figure. (b) Critical curves $LC = T_0(LC_{-1})$. The regions Z_k represent the set of point having k distinct pre-images. The points of $LC^{(a)}$ have four pre-images, two of which merge on $LC^{(a)}_{-1}$; the points of $LC^{(b)}$ have four pre-images, two of them merge on the left branch of $LC^{(b)}_{-1}$, the other two on the right branch of $LC^{(b)}_{-1}$. (c) Basins of attraction of a 2-cycle attracting node $\mathscr{A}_2$ on the a-axis and of the fixed point R^*. The white points belong to the basin $\mathscr{B}(R^*)$, the dark-grey points denote the basin $\mathscr{B}(\mathscr{A}_2)$ and the light-grey points belong to the basin of infinity (diverging trajectories). The repelling fixed points Q^*, P^* and S^* belong to the boundaries. In the enlargement of (c) the half-fractal structure of the frontier of the basins is shown, due to the pre-images of any rank of the small area U_0 in the region $V > 0$.

the critical curve LC_{-1} of T_0, and is also the line of symmetry of the parabola f, as the critical point C_{-1} of f has co-ordinate $a_{c_{-1}}$, $a_{c_{-1}} = \Gamma_1/2\Gamma_2$.

The proof of Property 3 is easily obtained by using the change of co-ordinate $b = a - \Gamma_1/2\Gamma_2$ in (21). We get a topologically conjugate map:

$$b' = -\Gamma_2 b^2 - \Gamma_2 V + \frac{\Delta - 1}{4\Gamma_2}, \qquad V' = \Gamma_2^2(\beta - 1)V^2 + 4\Gamma_2^2 b^2 V \tag{27}$$

which depends only on b^2.

We can also investigate whether "feasible trajectories" of the map exist. From an applicative point of view we are interested in bounded trajectories the points of which have $V \geqslant 0$ and $a > 0$. The second condition may probably be obtained if the parameters are such that $a^*_Q \gg 0$. This is not a rigorous proof, but an empirical result, shown in the examples of this paper, which has a theoretical support on the one-dimensional restriction to the a-axis. Moreover, from Property 4 follows that the map is suitable for applications.

Property 4 (Feasible trajectories of T_0). *Let $\beta \geqslant 1$. Then a point (a, V) with $V > 0$ is mapped by T_0 into a point (a', V') with $V' > 0$.*

In other words, a point (a, V) having $V < 0$ cannot have a feasible point as rank-1 pre-image, and this means that all its pre-images, of any rank, are in the negative half-plane $V < 0$. This property is useful to understand the global structure of the basins of attraction. Even if we are interested in the portion belonging to the half-plane $V \geqslant 0$, the changes in the structure of the basins depend on the global properties of the map in the whole plane. In particular on the number and position of the rank-1 pre-images of a point (a', V') by backward application of T_0. To this scope we have to determine the critical curves of the map. From the Jacobian matrix given in Appendix A it is easy to see that the locus Det $J(a, V) = 0$ is given by two curves, which represent, in our case, two branches of LC_{-1}, that is $LC_{-1} = LC_{-1}^{(a)} \cup LC_{-1}^{(b)}$ where

$$LC_{-1}^{(a)} : a = \frac{\Gamma_1}{2\Gamma_2} \quad \text{and} \quad LC_{-1}^{(b)} : V = \frac{(\Gamma_1 - 2\Gamma_2 a)^2}{2\Gamma_2^2(3-\beta)}. \tag{28}$$

The first curve is the symmetry line (26) of the basin, the second one is a parabola with vertex on the a-axis, in the critical point C_{-1} of the map f. We note that $LC_{-1}^{(a)}$ intersects the trapping axis in the critical point C_{-1}, while $LC_{-1}^{(b)}$ is tangent to that axis in C_{-1} (an example is shown in Fig. 1(a)). The images of these curves under the map T_0 give the two branches of LC, $LC = T_0(LC_{-1}) = LC^{(a)} \cup LC^{(b)}$. The branch $LC^{(a)}$ of equation

$$LC^{(a)} : V = (\beta - 1)\left(a - \frac{\Gamma_1^2 - 4\Gamma_0\Gamma_2}{4\Gamma_2}\right)^2 \tag{29}$$

is a convex parabola, when $\beta > 1$, with vertex on the a-axis in the critical point C of the map f, of coordinate $a_C = f(a_{C_{-1}}) = (\Gamma_1^2 - 4\Gamma_0\Gamma_2)/4\Gamma_2$, while for $\beta = 1$ the curve degenerates into the a-axis $V = 0$. The branch $LC^{(b)}$ of equation

$$LC^{(b)} : \begin{cases} V = \frac{4}{5-\beta}\left(a - \frac{\Gamma_1^2 - 4\Gamma_0\Gamma_2}{4\Gamma_2}\right)^2 \\ a \leqslant a_C = \frac{\Gamma_1^2 - 4\Gamma_0\Gamma_2}{4\Gamma_2} \end{cases} \tag{30}$$

is a semi-parabola with vertex on the a-axis, again in the critical point C of f, as shown in Fig. 1(b).

The portions of phase plane bounded by the critical curves $LC^{(a)}$ and $LC^{(b)}$ are regions Z_j, $j \in \{0, 2, 4\}$, the points of which have j different rank-1 pre-images. This can be seen by computing the rank-1 pre-images by $(T_0)^{-1}$ of a generic point of the plane. Given a point $p = (a', V')$, its rank-1 pre-images are the points $(b + (\Gamma_1/2\Gamma_2), V)$ where (b, V) are the real solutions of the algebraic system

$$-\Gamma_2 b^2 - \Gamma_2 V + \frac{\Delta - 1}{4\Gamma_2} = a' - \frac{\Gamma_1}{2\Gamma_2}, \qquad \Gamma_2^2(\beta - 1)V^2 + 4\Gamma_2^2 b^2 V = V'. \tag{31}$$

The system (31) may have 0, 2 or 4 solutions, which can be explicitly written, as shown in Appendix B. As a consequence we have that the portion of plane between $LC^{(a)}$ and $LC^{(b)}$ is a region Z_4 (see Fig. 1(b)). The region below the curve $LC^{(a)}$ is a region Z_2. The remaining portion of plane, bounded by $LC^{(b)}$ and a part of $LC^{(a)}$ (the one on the right of the point C) is a region Z_0.

From Fig. 1(c) it is also immediately evident the different structure which characterizes the basins in the region $V > 0$ with respect to those in the region $V < 0$. Besides Property 3 (which is peculiar of the map under study), we recall here another important property of any basin of attraction $\mathscr{B}$, that is, the boundary, or frontier, say $\mathscr{F} = \partial\mathscr{B}$, is backward invariant, which means invariant by inverse iterations of the map, including all the different inverses. Thus a frontier $\mathscr{F}$ includes the stable sets of all the cycles belonging to $\mathscr{F}$. In Fig. 1(c) the frontier $\mathscr{F} = \partial\mathscr{B}(\infty)$ includes the repelling fixed points S^* (see Appendix A), Q^* and P^*, and their stable sets. Note that if a point is a repelling node (as Q^* for example), then its stable set is given by the set of all its pre-images of any rank ($W^s = \bigcup_{n>0} T_0^{-n}(Q^*)$). The upper boundary of the frontiers of $\mathscr{B}(R^*)$ and $\mathscr{B}(\mathscr{A}_2)$ in the region $V > 0$ have a smooth shape. This is due to the fact that only a few cycles

exist on the frontier in the region $V > 0$ (on which the pre-images of points of the frontiers accumulate), and to the existence of the region Z_0 whose points have no pre-images. On the contrary, the frontiers of the two basins in the region $V < 0$ have an "half-fractal" structure, i.e. are made up of smooth arcs having a self-similar structure which accumulate on a Cantor set of points which includes repelling cycles of T_0 of any order. This can be explained as follows. We recall that the whole half-plane $V < 0$ belongs to Z_2, that is, any point in this region has two rank-one pre-images, which are one on the right and one on the left of $LC_{-1}^{(a)}$, the symmetry line. For a point $p = (a, V)$ with $V < 0$, let $(T_0)_1^{-1}(p)$ be the rank-1 pre-image on the right, and $(T_0)_2^{-1}(p)$ the one on the left, of $LC_{-1}^{(a)}$. From Property 4 we have that both these rank-1 pre-images are again in the half-plane $V < 0$. Thus we can iteratively repeat the application of the two inverses $(T_0)_1^{-1}$ and $(T_0)_2^{-1}$ to all the points so obtained, and also to a portion in this region, noticing that starting from points in $\mathscr{B}(R^*)$ or in $\mathscr{B}(\mathscr{A}_2$ in the region $V < 0$ we cannot exit from these basins. This mechanism can be used to show that infinitely many repelling cycles of T_0, of any order, exist on the boundaries. In particular the fixed points Q^* and P^* on the a-axis have infinitely many pre-images on the frontiers below the invariant line, and these pre-images also have the fixed points as limit sets. That is, pre-images of the fixed points can be found as near to the fixed points as we want. This means that both the fixed points Q^* and P^* are snap-back-repellers (see [15,13]) and chaotic dynamics exist on the frontiers of the basins (but not inside). It is also easy to compute numerically homoclinic points of Q^* and homoclinic points of P^*, as the inverses are explicitly known, and we can choose particular sequences in the arborescent structure of inverses, more suitable to find the homoclinic points. For example, consider the rank-1 pre-image $Q_{-1}^* = (a_{Q_{-1}}, 0)$ where $a_{Q_{-1}} = (\Gamma_1 + 1 + \sqrt{\Delta})/2\Gamma_2$, then applying iteratively the inverse which gives points on the left, $\bigcup_{n>0}(T_0)_2^{-n}(Q_{-1}^*)$, we get an homoclinic orbit of Q^*. Similarly, considering the rank-1 pre-image of P^* on the a-axis, say P_{-1}^*, then $\bigcup_{n>0}(T_0)_1^{-n}(P_{-1}^*)$ gives an homoclinic orbit of P^*. We remark that by repeating iteratively any kind of composition of the two inverses $(T_0)_1^{-1}$ and $(T_0)_2^{-1}$, all the cycles of any order of the frontiers can be detected. Although this is not of direct interest in the applicative model under study (for which only the basins in the region $V > 0$ are to be considered), we can give reason of the half-fractal structure of the basins below the a-axis. The smooth arcs come from the basin $\mathscr{B}(R^*)$. In the enlargement of Fig. 1(c), an arrow shows a region denoted by U_0 above the a-axis, bounded by an arc of critical curve $LC^{(a)}$ and a portion of $\partial\mathscr{B}(R^*)$. The pre-images $U_{-1} = (T_0)_1^{-1}(U_0) \cup (T_0)_2^{-1}(U_0)$ give rise to the two regions connected on $LC_{-1}^{(a)}$, the two white portions having the shape of a "crescent". On its turn the region U_{-1} has an arborescent sequence of pre-images which gives rise to the half-fractal shape of the frontiers. We use the term "half" in characterizing this kind of frontier because we have the smooth arcs which accumulate in a self-similar shape on a repelling Cantor set. As we shall see in Section 5.2, the absence of smooth arcs gives rise to a "fractal" frontier.

5.1. Simply-connected, multiply-connected and disconnected basins

As we can see from Fig. 1(c), the white points belonging to the basin $\mathscr{B}(R^*)$ in the half-plane $V > 0$ we are interested in, constitute a simply-connected region, wide enough to consider this case quite suitable for an applicative interpretation, i.e. quite good also from a global point of view. Let us assume, for example, that the state of our system is near the equilibrium R^*, which is locally stable. We expect that the phase point will converge to the equilibrium, and if some exogenous event (a shock) happens, which changes the state of the system, putting it not far from the previous state, the basin is wide enough to think that we shall not go out of the basin of attraction. After the shock the iterations will continue to converge to the stable equilibrium starting from the new position. However the situation is often quite different, and even if a fixed point (or a different attractor) is locally stable, its basin may be not wide and not "robust" with respect to perturbations of the state.

An example is shown in Fig. 2(d), obtained with the same parameter values used in Fig. 1(c) except for a small increase in the value of λ. In Fig. 2(d) the fixed point R^* is still attracting but now the white points (belonging to its basin of attraction) are located in small "islands", although infinitely many in number. It is clear that a small shock applied to a point in the basin $\mathscr{B}(R^*)$ is likely to bring the point out of the basin, and from the new state the trajectory will be divergent. We remark again that what is changed from the situation in Fig. 1(c) to that of Fig. 2(d) is only the global structure of the basin $\mathscr{B}(R^*)$ and not the local character of the fixed point. On increasing λ from 0.5 to 0.57 several global bifurcations occur, which can

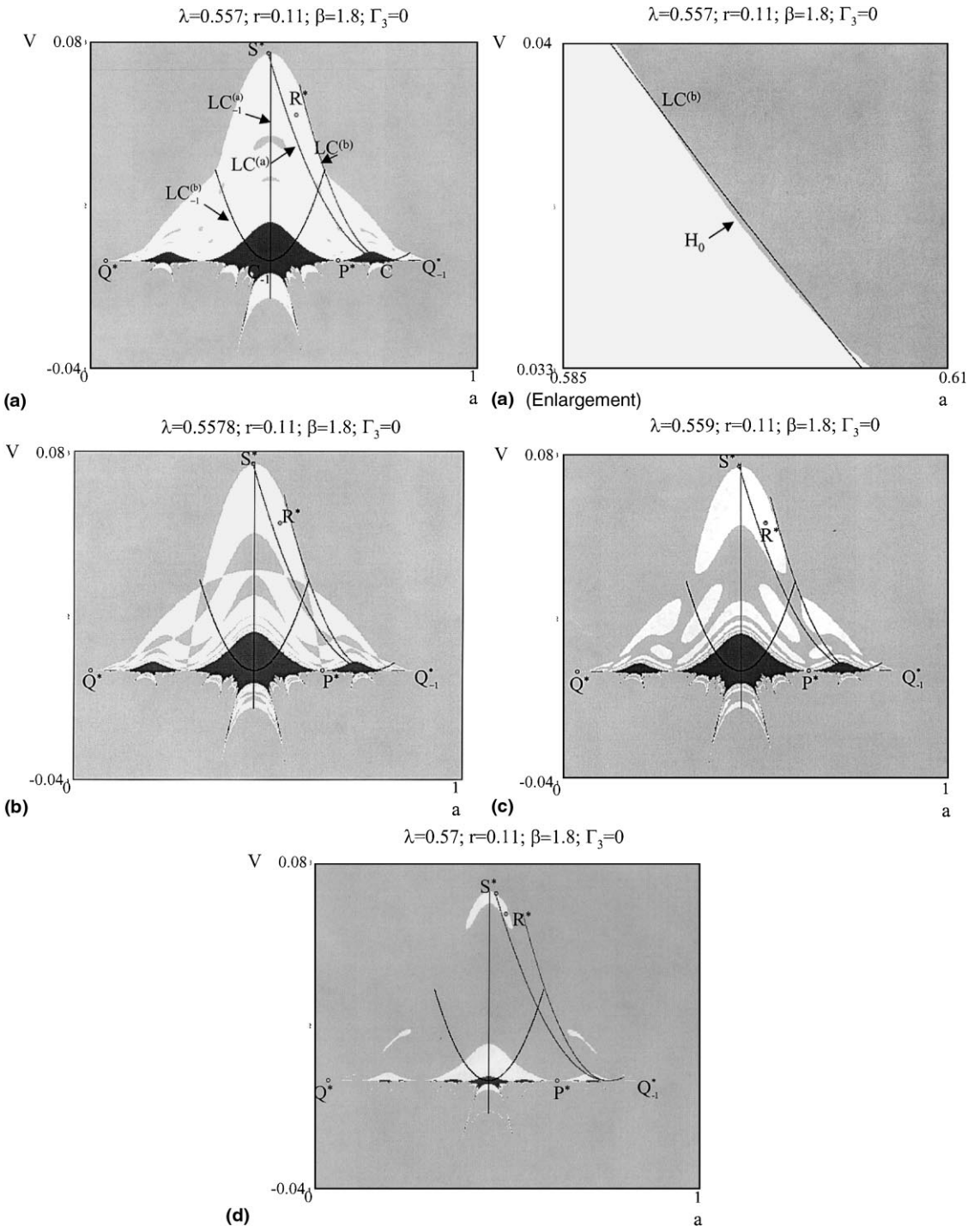

Fig. 2. Bifurcations of the basin $\mathscr{B}(R^*)$. (a) After the contact of $LC^{(b)}$ with the portion of frontier which separates the basins $\mathscr{B}(R^*)$ and $\mathscr{B}(\infty)$, the region H_0 enters in Z_4, as shown in the enlargement. The pre-images of H_0 give "holes" of light-grey points nested inside the basin the basin $\mathscr{B}(R^*)$, which is multiply-connected. (b) The light-grey holes inside $\mathscr{B}(R^*)$ are increased in size and in number and are all quite near to each other. (c) After the global bifurcation at which all the existing holes come in contact to each other, $\mathscr{B}(R^*)$ is made up of disconnected "islands". (d) The fixed point R^* is still attracting but now its basin (the white points) is quite reduced.

easily be explained by using the critical curves. As λ increases from 0.5 a portion of the frontier which separates the basins $\mathscr{B}(R^*)$ and $\mathscr{B}(\infty)$ approaches the critical curve $LC^{(b)}$, which separates the region Z_0 from Z_4. The first bifurcation occurs when the frontier becomes tangent to the critical curve, and after the frontier will cross the critical curve. This bifurcation causes the transition of the basin $\mathscr{B}(R^*)$ above the a-axis from simply-connected to multiply-connected. In fact, soon after the crossing, a portion of $\mathscr{B}(\infty)$ which was previously in Z_0 (and thus without pre-images) enters in Z_4 (and thus will have pre-images). This portion is denoted as H_0 in the enlargement of Fig. 2(a), bounded by an arc of $LC^{(b)}$ and a portion of frontier. As H_0 belongs to the basin $\mathscr{B}(\infty)$ of divergent trajectories, the same is true for all the points belonging to its pre-images, $\bigcup_{n>0} T^{-n}(H_0)$, giving "holes" of light-grey points nested insides the basin $\mathscr{B}(R^*)$, which is now a multiply-connected basin. The rank-1 pre-images of H_0 include a hole through $LC^{(b)}_{-1}$, and then any hole has either two or four distinct rank-1 pre-images, depending on the region Z_2 or Z_4 to which it belongs, while the holes falling in Z_0 have no further pre-images. Only a few of them are visible in Fig. 2(a).

As λ increases, the size of the holes $\bigcup_{n>0} T^{-n}(H_0)$ also increases, and new contacts of some of them with branches of LC inside $\mathscr{B}(R^*)$ also occur, which cause an increase of the number of the holes, as new "germs" on LC_{-1} are created from such contacts, giving rise to new holes. This mechanism of global bifurcations is typical in non-invertible maps of the plane, as described in [16,1,2].

In Fig. 2(b) we can see that all the light-grey holes inside $\mathscr{B}(R^*)$ are quite near to each other, and another important global bifurcation is approaching, at which all the existing holes will come in contact to each other, all at the same time (bifurcation value), after which the grey "islands" will "open into the sea" $\mathscr{B}(\infty)$, following the picturesque description introduced in [16], leaving disconnected "islands" $\mathscr{B}(R^*)$, as shown in Fig. 2(c).

As λ is increased further, the islands constituting the basin of the fixed point decrease in size, leading to the situation already commented of Fig. 2(d). We are certainly allowed to say that now the "locally stable" fixed point R^* is "almost globally unstable".

5.2. Multi-multi-stability

In this section we consider a special case for the map T_0 which is obtained when $\beta = 1$. As shown in (29), in this case the critical curve $LC^{(a)}$ merges with the a-axis, and the region Z_4 becomes wider. In particular the fact that now all the points of the a-axis are critical points has several consequences for the dynamics. Note that all the points of the interval $[-\infty, C]$, where C is the critical point of f, belong to the boundary of the region Z_4, and besides the two distinct pre-images on the line itself, they have two more coincident rank-one pre-images on the line of symmetry $LC^{(a)}_{-1}$. Those of the interval $[C, +\infty]$ have only the two coincident rank-one pre-images on the line of symmetry. The region Z_2 is the half-plane $V < 0$. The qualitative changes with respect to the case considered in the previous section, especially in the basins of attractions, are immediately evident from Fig. 3(a).

The parameters are the same as those considered in Fig. 1(c) except for the parameter β, which is now equal to 1. These two maps have the same cycles, in particular the same fixed points with the same kind of local stability, but globally different behaviour. The colours in the two pictures have the same meaning (white points give the basin $\mathscr{B}(R^*)$, dark grey points the basin $\mathscr{B}(\mathscr{A}_2)$ and the light grey the basin $\mathscr{B}(\infty)$), and perhaps it is surprising how wide is the basin of the 2-cycle on the a-axis (i.e. many points with positive variance will ultimately converge to a state with zero variance). The basin $\mathscr{B}(\mathscr{A}_2)$ has such a structure because the "immediate basin" around the trapping line $V = 0$ has now a big portion in the region Z_4 and more pre-images than in the other case exist. The portion of this basin in the half-plane $V > 0$ may be considered disconnected, made up of infinitely many components of "quadrilateral shape", but with connected closure, and the points connecting these portions, the extrema of the quadrilateral regions, are all *pre-images of any rank of the repelling fixed point* P^*. This fixed point has one rank-1 pre-image in itself, another rank-1 pre-image on the a-axis, called $P^*_{-1,1}$ in Fig. 3(a), and two merging rank-1 pre-images in the point $P^*_{-1,2}$ of the symmetry line. This last point is internal to Z_4 and thus has four distinct rank-1 pre-images, all in the feasible half-plane $V > 0$, and so on. In fact, it is easy to see that besides Property 4, now a stronger property holds:

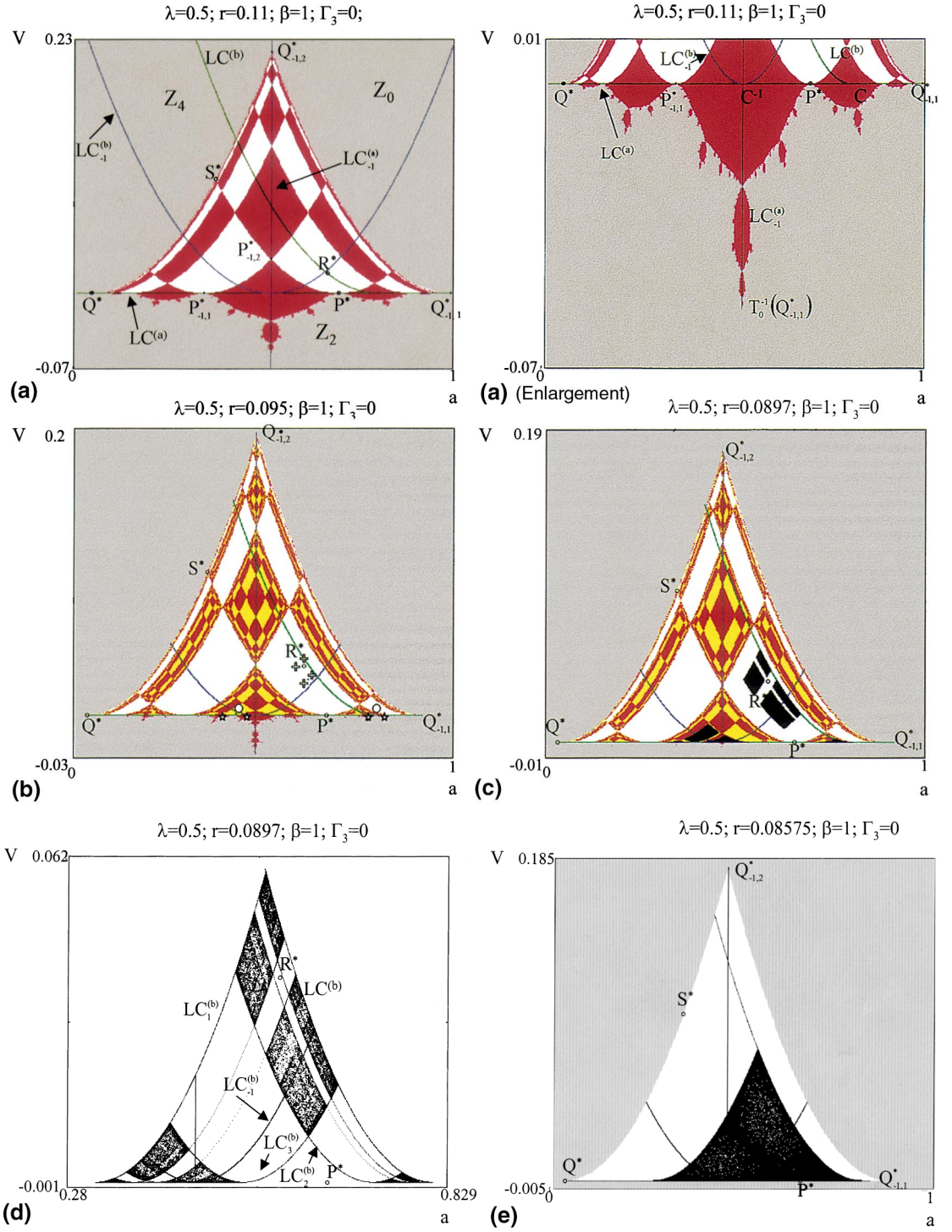

Fig. 3. (a) The white points belong to the basin $\mathscr{B}(R^*)$, the red points denote the basin $\mathscr{B}(\mathscr{A}_2)$ of the 2-cycle on the a-axis, and the grey points $\mathscr{B}(\infty)$. The portion of the basin $\mathscr{B}(\mathscr{A}_2)$ in the region $V > 0$ is made up of infinitely many components of "quadrilateral shape", whose extrema are pre-images of the repelling fixed point P^*. In the enlargement of (a) it is shown the portion of the basin $\mathscr{B}(\mathscr{A}_2)$ in the region $V < 0$ which is fractal. (b) A 4-cycle $\mathscr{A}_4$ attracting node (marked with stars) exists on the a-axis (born by flip-bifurcation). Other two attracting cycles exist: a 2-cycle $\mathscr{A}'_2$, marked with circles, just above the a-axis, and a 4-cycle $\mathscr{A}'_4$, marked with cross, near the fixed point R^*, now repelling. The points inside the "old quadrilateral portions" of Fig. 3(a) now are divided into points belonging to $\mathscr{B}(A_4)$ and to $\mathscr{B}(A'_2)$, again in basins having a quadrilateral shape (self-similar structure). (c) There are three co-existing different attractors, with chaotic dynamics: a 4-band chaotic attractor around the repelling fixed point R^*, a 2-band chaotic attractor near the a-axis (all in the positive region), and a 4-pieces chaotic attractor having one side on the a-axis. (d) All the chaotic areas of Fig. 3(c) belong to an absorbing area bounded by the critical arcs $LC_k^{(b)} = T_0^k\left(LC_{-1}^{(b)}\right)$, $k = 1, 2, \ldots, 7$. (e) Single chaotic area, bounded by arcs of LC and LC_1.

Property 5. *Let $\beta = 1$ in the map T_0. Then all the rank-1 pre-images of a point (a, V) with $V > 0$ (resp. $V < 0$) are points belonging to the half-plane $V > 0$ (resp. $V < 0$).*

As a consequence of this property we have that no white point can exist below the a-axis, that is, the basin $\mathscr{B}(\mathscr{R}^*)$ of the stable fixed point is necessarily in the feasible region $V > 0$.

As already remarked in Section 5, there is a great difference in the shape of the frontiers in the two half-planes: those above the a-axis are smooth, and those below are fractal (now true fractal). It is quite evident the similarity of the frontier of the basin in the region $V < 0$ (see the enlargement of Fig. 3(a)) with the fractal set obtained for the basin of the complex map $z' = z^2 - 1$ (see, for example, [17]). The fixed points Q^* and P^* have homoclinic points, and the same is true for all the infinitely many repelling cycles on that frontier in the region $V < 0$.

As the parameter r is decreased, we increase the non-linear effects in the one-dimensional map f, the attracting 2-cycle undergoes a flip-bifurcation, and an attracting 4-cycle appears. As we know from Property 2, this is also a bifurcation for the map T_0, of co-dimension two. The result in our case is that the 2-cycle $\mathscr{A}_2$ turns into a repelling node and a 4-cycle $\mathscr{A}_4$ attracting node appears on the a-axis, and, at the same time, another 2-cycle $\mathscr{A}'_2$ attracting node appears just above the a-axis (bifurcating from $\mathscr{A}_2$). Moreover, also the fixed point R^* becomes unstable, and attracting cycles are created near it. In Fig. 3(b) an attracting 4-cycle, say $\mathscr{A}'_4$, exists near the repelling focus $\mathscr{R}^*$. Reassuming, we have three co-existing attracting cycles: $\mathscr{A}'_2$ and $\mathscr{A}'_4$ in the positive half-plane and $\mathscr{A}_4$ on the a-axis. Their basin of attraction are shown in Fig. 3(b). It can be seen that the points inside the "old quadrilateral portions" (old basin $\mathscr{B}(\mathscr{A}_2)$) of Fig. 3(a) now are divided into points belonging to $\mathscr{B}(\mathscr{A}_4)$ and to $\mathscr{B}(\mathscr{A}'_2)$, again in basins having a quadrilateral shape (self-similar structure), the extrema of which are the pre-images of any rank of the repelling two cycle $\mathscr{A}_2$.

As r is further decreased several bifurcations lead to chaotic attractors. In Fig. 3(c) we show a situation in which there are three co-existing different attractors, with chaotic dynamics: a 4-band chaotic attractor around the repelling fixed point $\mathscr{R}^*$, a 2-band chaotic attractor near the a-axis (but all in the positive region), and a 4-pieces chaotic attractor having one side on the a-axis. As in the one-dimensional case the chaotic intervals are bounded by critical points, in the two-dimensional case we have absorbing areas and chaotic areas bounded by segments of critical curves. Following [1,2], by taking the segment of critical curve $LC_{-1}^{(b)}$ inside the area of the example given in Fig. 3(c), with a few images by T_0 we get an invariant area bounded by critical segments, shown in Fig. 3(d). With smaller segments of $LC_{-1}^{(b)}$ all the distinct pieces of chaotic areas are bounded by a few critical arcs. Then the chaotic areas increase in size, and shall merge into a single chaotic piece. An example is shown in Fig. 3(e). It is clear that now the state of the system is unpredictable. However, we can observe that such a state is not "completely" unknown, because we know its width, i.e. the boundary of the chaotic area. It means that even if we cannot predict the state of the system we know the possible width of its variations. For the a-values we know the range, say $[a_{\min}, a_{\max}]$ in which it is confined, and the same for the values of the variance, $V \in [V_{\min}, V_{\max}]$, and often this is already a good information.

The sequence in Fig. 3 commented above is associated with parameter values of the logistic map inside the period-2 "box" (see the "box-within-a-box" bifurcation structure described in [12], or the "window" in [14]), and we know that on decreasing r all the boxes associated with any cycle appear. Similar behaviour occurs also in the positive half-plane: several co-existing attracting cycles may exist, and transition to $k-$band chaotic attractors for any natural k. In Fig. 4 we show some situations occurring inside the "period-3 box".

In Fig. 4(a) we have observed two attractors: a 3-cycle on the a-axis and a 3-cycle around the repelling $\mathscr{R}^*$. It is worth noting that inside the area previously occupied by the chaotic attractor now a chaotic repellor survives (which are zero-measure invariant sets with chaotic dynamics, containing repelling cycles and their stable sets) and this is the cause of the complex structure of the basins of the two 3-cycles, as shown in Fig. 4(a) and in its enlargement. Note that although we have only two simple attractors (two cycles of period 3), and a wide set of points with bounded trajectories in the positive half-plane, there are several regions in which we cannot predict the asymptotic behaviour for a generic initial condition. In fact, apart from the immediate basins of the two cycles and their first pre-images of low rank, the areas belonging to the different basins become smaller and smaller accumulating in the points of the repelling

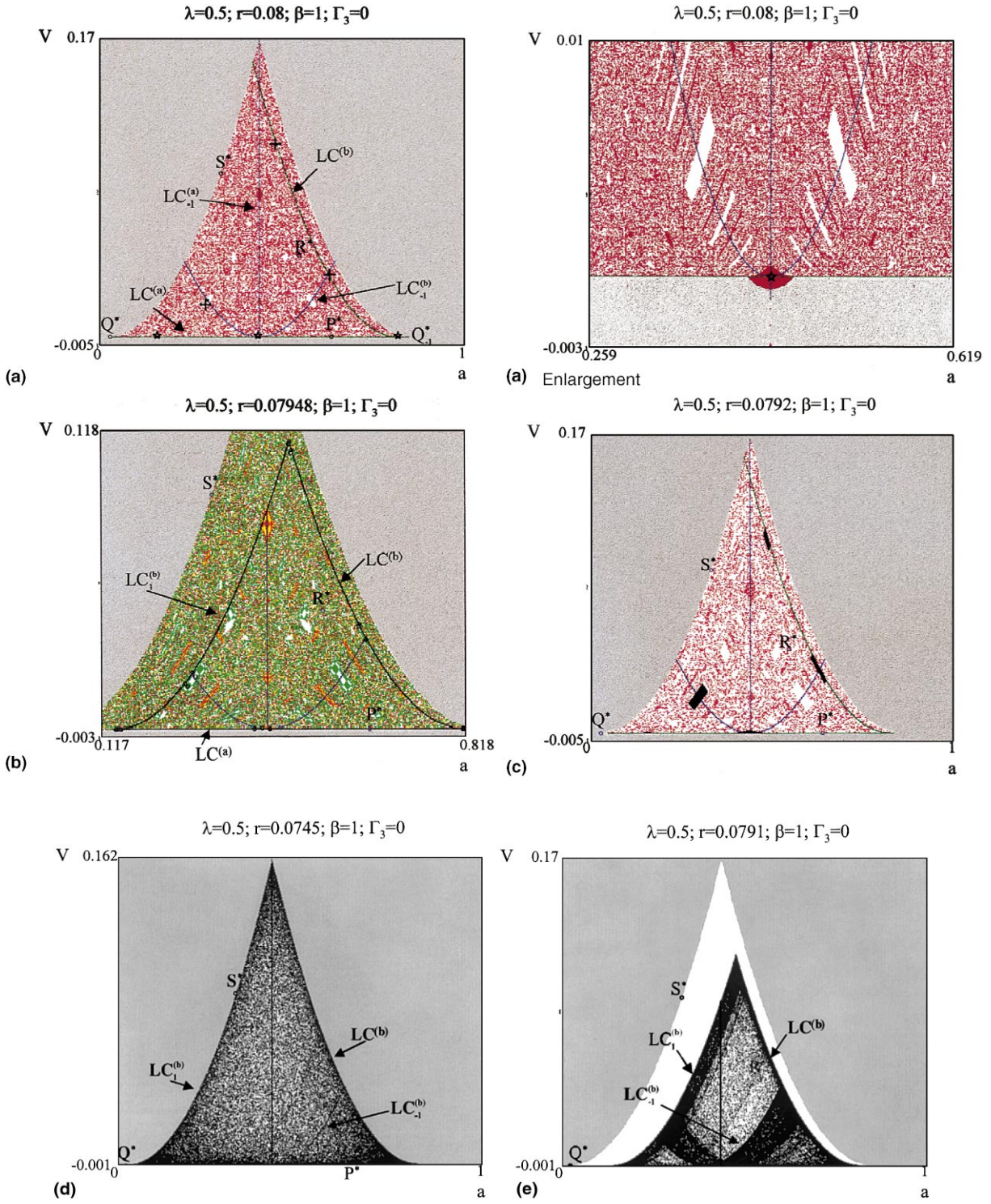

Fig. 4. Period-3 box. (a) Basins of two different attractors: a 3-cycle on the a-axis, marked with stars, and a 3-cycle around the repelling point R^*, marked with cross. The areas belonging to the different basins (red and white points) are intermingled in a chaotic (fractal) way, as shown in the Enlargement. (b) We have four different attractors: a 6-cycle on the a-axis, a 3-cycle just above the a-axis and two 6-cycles with positive variance. Their basins of attraction (white, green, yellow and red points) are chaotically intermingled. All these cycles belong to the absorbing area bounded by three critical arcs. (c) Two co-existing attractors: a 3-band chaotic attractor in the region $V > 0$ and a 3-pieces chaotic attractor having one side on the a-axis. (d) One-piece chaotic attractor, bounded by three arcs of critical curves. (e) The chaotic area completely fills its basin.

Cantor sets, and thus are intermingled in a chaotic (fractal) way. Clearly in this situation there is also unpredictability with respect to an exogenous shock, as perturbing a state we can no longer say whether the asymptotic behaviour will be the same or will change.

As before, when the flip bifurcation of the 3-cycle on the a-axis occurs, giving rise to an attracting 6-cycle on the a-axis, then (due to the bifurcation of both the eigenvalues) also an attracting 3-cycle with positive variance appears. Moreover, other bifurcations of the two-dimensional map lead to two other different 6-cycles with positive variance, and in the absorbing area of Fig. 4(b) there are such *four different attracting sets*. It is clear that their basins of attraction are chaotically intermingled.

As expected, we get chaotic regions as r is decreased further. In Fig. 4(c) we have two co-existing chaotic attractors: a 3-band chaotic pieces in the region $V > 0$ and 3-cyclical chaotic pieces having one side on the a-axis. These will turn into a one-piece chaotic attractor, bounded by three arcs of critical curves, as shown in Fig. 4(d).

On decreasing r for the one-dimensional map f all the dynamics occur, up to $\Delta = 9$ (i.e. $\mu = 4$ in the standard logistic), and this is the last value at which a bounded invariant interval exists. Similarly, the two-dimensional attracting sets belong to wider and wider absorbing areas, up to this last bifurcation, when the two-dimensional chaotic area completely fills its basin (as it occurs for the one-dimensional restriction), as shown in Fig. 4(e). Beyond this value the generic trajectory will be divergent.

6. Non-symmetric distribution case ($\Gamma_3 > 0$)

In this section we return to consider the complete model, the map T given in (18), in the generic case of non-symmetric distribution, which means that the parameter Γ_3 is positive (and small, as already remarked in Section 4). In this case we loose all the analytical results of Section 5. Only "guided" numerical investigations can be used. Being Γ_3 very close to zero, we can consider the map T as a slight perturbation of the map T_0 of the symmetric case. This will be evident from the examples described in this section.

We first note that the critical curves can be obtained numerically, by drawing the set Det $J(a, V) = 0$ which gives LC_{-1}. This curve now consists of two disjoint branches (perturbations of the two intersecting branches occurring in the symmetric case). In Fig. 5(a) we consider parameter values close to those used in Figs. 1 and 2 of Section 5.

Besides the critical curve $LC_{-1} = LC_{-1}^{(a)} \cup LC_{-1}^{(b)}$ also $LC = T\ (LC_{-1})$ is numerically computed, and its two branches are shown in Fig. 5(a). The branch $LC^{(a)}$ has a cusp point while the branch $LC^{(b)}$ has a parabolic shape. Moreover we compute numerically the distinct rank-1 pre-images of a point of the plane finding that the area enclosed by the critical curve $LC^{(a)}$ is a region Z_4, the region above $LC^{(b)}$ is Z_0 and the remaining region is Z_2.

Also the fixed points are numerically computed, solving the system in (20), which has four real solutions, called R^*, Q^*, P^* and S^* in Fig. 5(a). Only R^* is locally stable, the other three fixed points belong to the frontier $\mathscr{F}$ which separates the basin of R^* from the points having divergent trajectories (i.e. $\mathscr{F} = \partial\mathscr{B}(R^*) = \partial\mathscr{B}(\infty)$). Now the a-axis is no longer invariant, however we can still observe two different qualitative structures in the shape of $\mathscr{F}$. The lower part between Q^* and Q^*_{-1} (completely in Z_2) has still an half-fractal shape, which can be explained by using arguments similar to those used in Section 5. Whereas the upper part of $\mathscr{F}$ has a smooth shape. The grey points of Fig. 5(a) give the basin $\mathscr{B}(\infty)$, while the white region is the locus of points having bounded trajectories. As besides the fixed point R^* we have not observed any other attracting set for T, we assume that the white region is $\mathscr{B}(R^*)$.

The dynamic behaviour of T as the parameters are varied from the case of Fig. 5(a) are very similar to those observed in the symmetric case. Either increasing λ or decreasing r the global bifurcations of the basin of bounded trajectories occur, due to contacts with the critical curves, changing the simply-connected basin into a multiply-connected and then into a disconnected one. The only difference is in the attracting set which, instead of the fixed point R^*, may be a closed invariant curve Γ^* born at the supercritical Neimark–Hopf bifurcation of R^* (turned into repelling focus). In Fig. 5(b) we can see such closed invariant attracting curve Γ^* (we have chosen to show what occurs on decreasing r). A contact bifurcation between $\mathscr{F}$ and the critical curve $LC^{(b)}$, causing the first global bifurcation of the basin, has already occurred, and then the crossing creates a portion H_0 of the basin $\mathscr{B}(\infty)$ which belongs now to Z_2 (previously in Z_0), see the

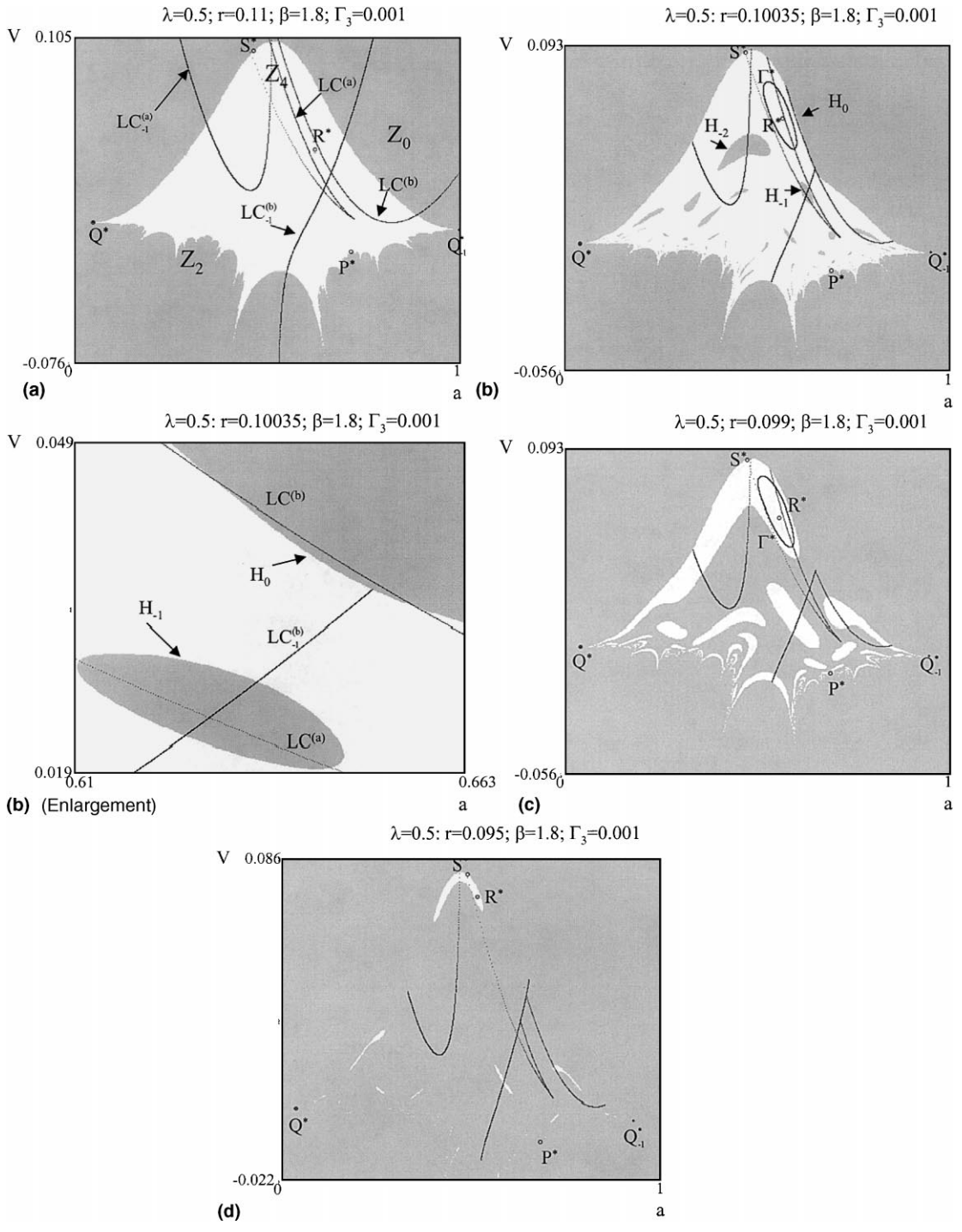

Fig. 5. The non-symmetric distribution case: multiply-connected basins. The parameters values are initially the same as in Fig. 1(c), but $\Gamma_3 = 0.001$. We decrease the interest rate r. (a) The grey points have divergent trajectories, the white ones belong to the basin of the attracting fixed point R^*. Q^*, P^* and S^* are repelling fixed points on the basin boundary. The branch $LC^{(a)}$ has a cusp point while the branch $LC^{(b)}$ has a parabolic shape. The regions Z_0, Z_2 and Z_4 are also shown. The basin $\mathscr{B}(R^*)$ is simply-connected and its frontier has a smooth upper part and a half-fractal lower part. (b) A supercritical Neymark–Hopf bifurcation of R^* caused the birth of the closed invariant curve Γ^*. A contact bifurcation between the frontier $\mathscr{F}$ and the critical curve $LC^{(b)}$ has already occurred, and the crossing creates a portion H_0 of the basin $\mathscr{B}(\infty)$, previously in Z_0, which belongs now to Z_2, shown in the enlargement. Then infinitely many pre-images of H_0 of any rank exist, giving "holes" of $\mathscr{B}(\infty)$ within the basin $\mathscr{B}(\Gamma^*)$. In the enlargement we see H_{-1}. (c) The "holes" open into the sea, leaving a disconnected basins $\mathscr{B}(\Gamma^*)$. (d) The closed curve disappears leaving an attracting fixed point R^*, whose basin is now quite reduced.

enlargement of Fig. 5(b). Then infinitely many pre-images of H_0 of any rank exist, giving "holes" of $\mathscr{B}(\infty)$ within the basin $\mathscr{B}(\Gamma^*)$. As r is decreased further the holes increase in size as well as in number, due to other contacts of the boundaries of the holes with the branches of critical curves $LC^{(a)}$ and $LC^{(b)}$ inside the basin $\mathscr{B}(\Gamma^*)$. The holes will then approach each other until a global bifurcation occurs, at which all of them will come in touch and then "the holes will open into the sea", leaving a disconnected basin $\mathscr{B}(\Gamma^*)$. An example is shown in Fig. 5(c). A particular behaviour is now observed on decreasing r: the closed invariant attracting curve Γ^* decreases in size, approaching the repelling focus R^*, and a "reverse" Neimark–Hopf bifurcation occurs: the closed curve disappears leaving an attracting fixed point R^*. In Fig. 5(d) we are in such a situation. Note that now the immediate basin of R^*, say $\mathscr{B}_0(R^*)$, (i.e. the simply connected area of the basin including the attracting set) is very small, and on its frontier there is only the saddle S^*. We argue that the frontier $\partial\mathscr{B}_0(R^*)$ of the immediate basin is the local stable set of the saddle S^*, and then the total basin is made up of all its pre-images of any rank, $\mathscr{B}(R^*) = \bigcup_{n \geqslant 0} T^{-n}(\mathscr{B}_0(R^*))$, which are infinitely many (even if only a few of them can be observed in Fig. 5(d)), and accumulating on all the existing repelling cycles of T.

Comparing the dynamics of the map in the cases shown in Fig. 5(a) and (d), where T has a unique attracting set, the stable fixed point R^*, we are led to comments similar to those presented in Section 5.1. Attention must be paid when only the *local* stability of an attractor is analyzed, because we may be in a *globally robust* situation as that of Fig. 5(a) or in a situation in which the locally stable fixed point may be considered as *almost globally unstable*, as that in Fig. 5(d).

We end the comments of this example by noticing that if r is further decreased, the fixed point R^* (which turns into an attracting node) and the saddle S^* will come close to each other, and will merge together at a "reverse" saddle-node bifurcation which make disappear these two fixed points. Then the generic trajectory has been observed to be divergent.

Finally we close this section showing the dynamics of T when we perturb the particular case presented in Section 5.2, considering $\Gamma_3 = 0.001$. In Fig. 6(a) the numerically computed critical curves LC_{-1} and LC are drawn, each of which is made up of two distinct branches, and also the fixed points R^*, Q^*, P^* and S^*. As above, only R^* is locally stable while the other three fixed points belong to the frontier $\mathscr{F}$ which separates the basin of R^* from the points having divergent trajectories.

Also now the area enclosed by the critical curve $LC^{(a)}$ is a region Z_4, the region above $LC^{(b)}$ is Z_0 while Z_2 is the remaining region. We can observe that Z_4 is a wide region (a perturbation of the one in Fig. 3(a)), and now it includes the fixed point Q^*. Then this fixed point has four distinct rank-1 pre-images, one in itself and the points $Q^*_{-1,1}$, $Q^*_{-1,2}$, $Q^*_{-1,3}$ shown in Fig. 6(a), the last two of which belong to Z_0 and have no other pre-images, while $Q^*_{-1,1}$ belongs to Z_2 and has an arborescent sequence of pre-images, located in the lower part of $\mathscr{F}$ (where $\mathscr{F}$ appears to be half-fractal). In fact, as in the previous case, $\mathscr{F}$ is made up of two parts with different structures, the lower part between Q^* and $Q^*_{-1,1}$ which has an half-fractal shape, and the upper part which is smooth.

Again the multistability, which was a characteristic of the symmetric case, is lost after the symmetry-breaking, and we don't observe any other attractor besides the fixed point R^*, or the attracting set bifurcated from that point. Thus the white points of Fig. 6(a) are assumed to give $\mathscr{B}(R^*)$, while those in Fig. 6(b) belong to $\mathscr{B}(\Gamma^*)$, where Γ^* is an attracting closed invariant curve born via Neimark–Hopf bifurcation from R^*, on increasing λ. In the enlargement of Fig. 6(b) we see that the frontier $\mathscr{F}$, after a tangency with the lower branch of $LC^{(a)}$ crosses $LC^{(a)}$ and a portion H_0 of the basin $\mathscr{B}(\infty)$, previously in Z_2, now belongs to Z_4, giving rise to a couple of new pre-images, one on the right and one on the left of $LC^{(a)}_{-1}$, together constituting the hole H_{-1}. Thus the contact bifurcation of the frontier has caused the transition of the basin of bounded trajectories from simply-connected to multiply-connected, although now we have *only one hole* H_{-1} (because H_{-1} belongs to the region Z_0 and thus it has no other pre-images).

As λ is increased, frequency locking on the closed curve leads to an attracting 4-cycle for T and sequences of flip-bifurcations give rise to a 4-band chaotic attractor, belonging to an absorbing area of annular shape, and a contact bifurcation of the four pieces causes their reunion into a single chaotic attractor, as shown in Fig. 6(c). In the enlargement of that figure we see that the absorbing area is bounded by segments of critical curves $LC^{(b)}, LC^{(b)}_1, \ldots, LC^{(b)}_6$, obtained by iterating the small piece of arc of $LC^{(b)}_{-1}$ which crosses that area.

In Fig. 6(c) we can also see that the hole H_{-1} is increased in size and now crosses $LC^{(b)}$, thus a small portion of this hole enters Z_2, giving rise to new pre-images, called H_{-2} in that figure, but H_{-2} belongs to the region Z_0 and thus it has no other pre-images. However, the number of holes in the basin of bounded

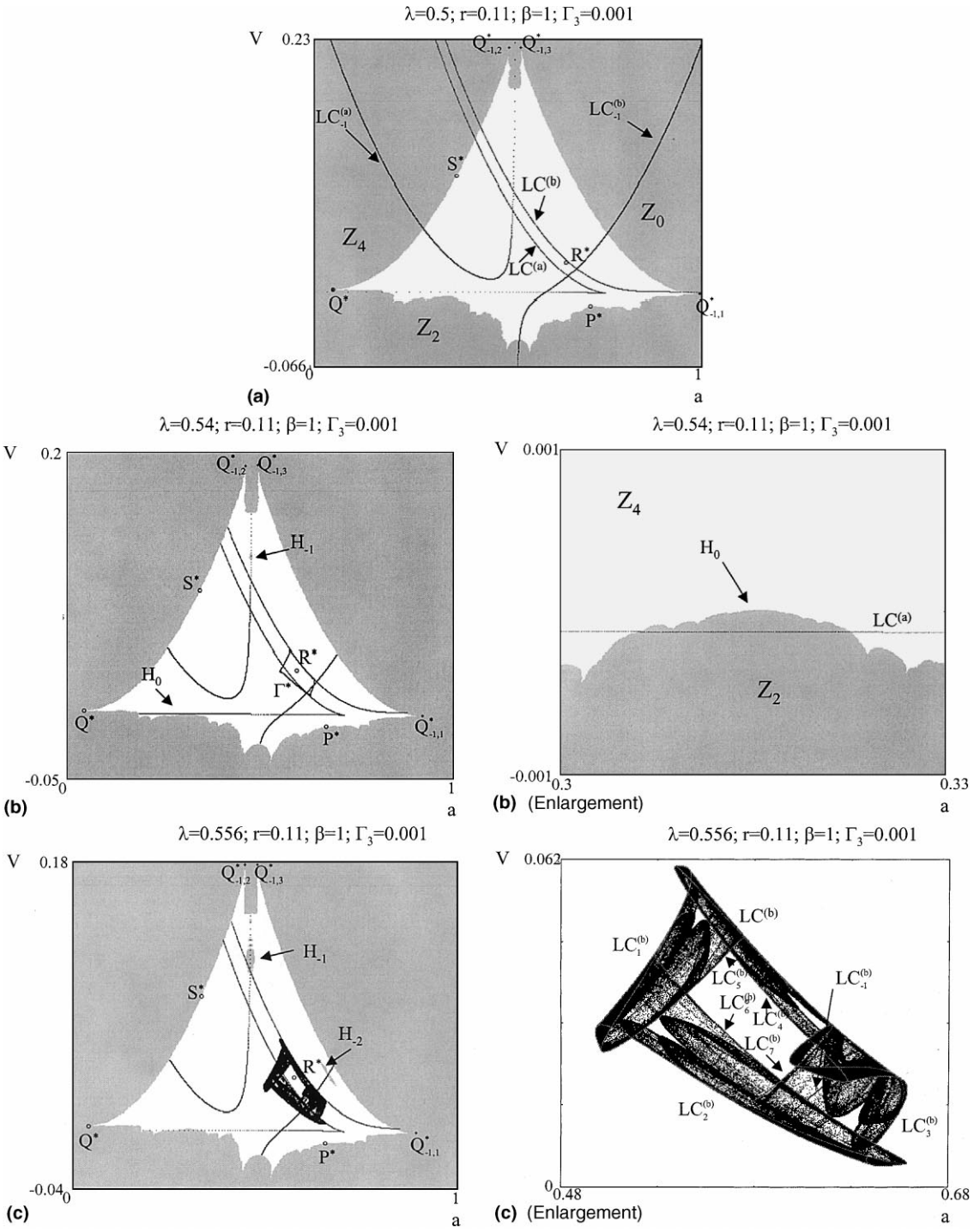

Fig. 6. Chaotic attractors in the non-symmetric case. As in Figs. 3 and 4, we set $\beta = 1$, but $\Gamma_3 = 0.001$. Chaotic attracting areas are obtained by increasing λ. (a) R^* is locally stable. The region Z_4 now is wider with respect to that of Fig. 5(a) and contains the fixed points Q^*. The points $Q^*_{-1,1}$, $Q^*_{-1,2}$, $Q^*_{-1,3}$ are the rank-1 pre-images of Q^*. $Q^*_{-1,1}$ belongs to Z_2 and has an arborescent sequence of pre-images, located in the lower part of the frontier $\mathscr{F}$ (where $\mathscr{F}$ appears to be half-fractal). In fact, as in the previous case, $\mathscr{F}$ is made up of two parts with different structures, the lower part between Q^* and $Q^*_{-1,1}$ which has an half-fractal shape, and the upper part which is smooth. (b) Γ^* is an attracting closed invariant curve born via Neimark–Hopf bifurcation from R^* and the white points belong to its basin. In the Enlargement we see that the frontier $\mathscr{F}$, after a tangency with the lower branch of $LC^{(a)}$ crosses $LC^{(a)}$ and a portion H_0 of the basin $\mathscr{B}(\infty)$, previously in Z_2, now belongs to Z_4, giving rise to the hole H_{-1}. Now we have *only one hole* H_{-1} (because H_{-1} belongs to the region Z_0 and thus it has no other pre-images). (c) Absorbing area of annular shape. In the Enlargement we see that the absorbing area is bounded by segments of critical curves $LC^{(b)}, LC^{(b)}_1, \ldots, LC^{(b)}_7$, obtained by iterating the small piece of arc of $LC^{(b)}_{-1}$ which crosses that area.

trajectories is increasing also due to new contacts of $\mathscr{F}$ with the lower part of $LC^{(a)}$, which is more clearly visible in the enlargement of Fig. 7(a).

Here we see that sequences of bifurcations in the attracting sets have led to a chaotic area, again bounded by a few segments of critical curves $LC_j^{(b)}$. As λ is further increased the chaotic area crosses also $LC_{-1}^{(a)}$ and the boundary of the chaotic area now includes also segments of $LC_j^{(a)}$. Also the holes approach and cross the upper branch of $LC^{(a)}$ having a portion which, from Z_2, enters Z_4 giving rise to new pre-images. The appearance of a portion of the hole H_{-1} in the region Z_4 is a bifurcation with more consequences than the previous ones because now the pre-images of any rank of this portion are not finite in number, but infinitely many, even if only a few of them are visible in Fig. 7(b) (for example, an infinite sequence of pre-images exists which gives smaller and smaller holes approaching the fixed point Q^* inside the region Z_4).

Several bifurcations are observed in the attracting sets on varying λ, appearance of boxes of stable cycles and their routes to chaos, and explosions in wider chaotic areas. In the last figure, Fig. 7(c), we see that the chaotic area is now very close to the frontier of its basin. As in fact a contact will occur, causing the transition of that chaotic attractor into a chaotic repellor, after which the generic trajectory is observed to be divergent. However, we remark that this example corresponds to what is generally observed in

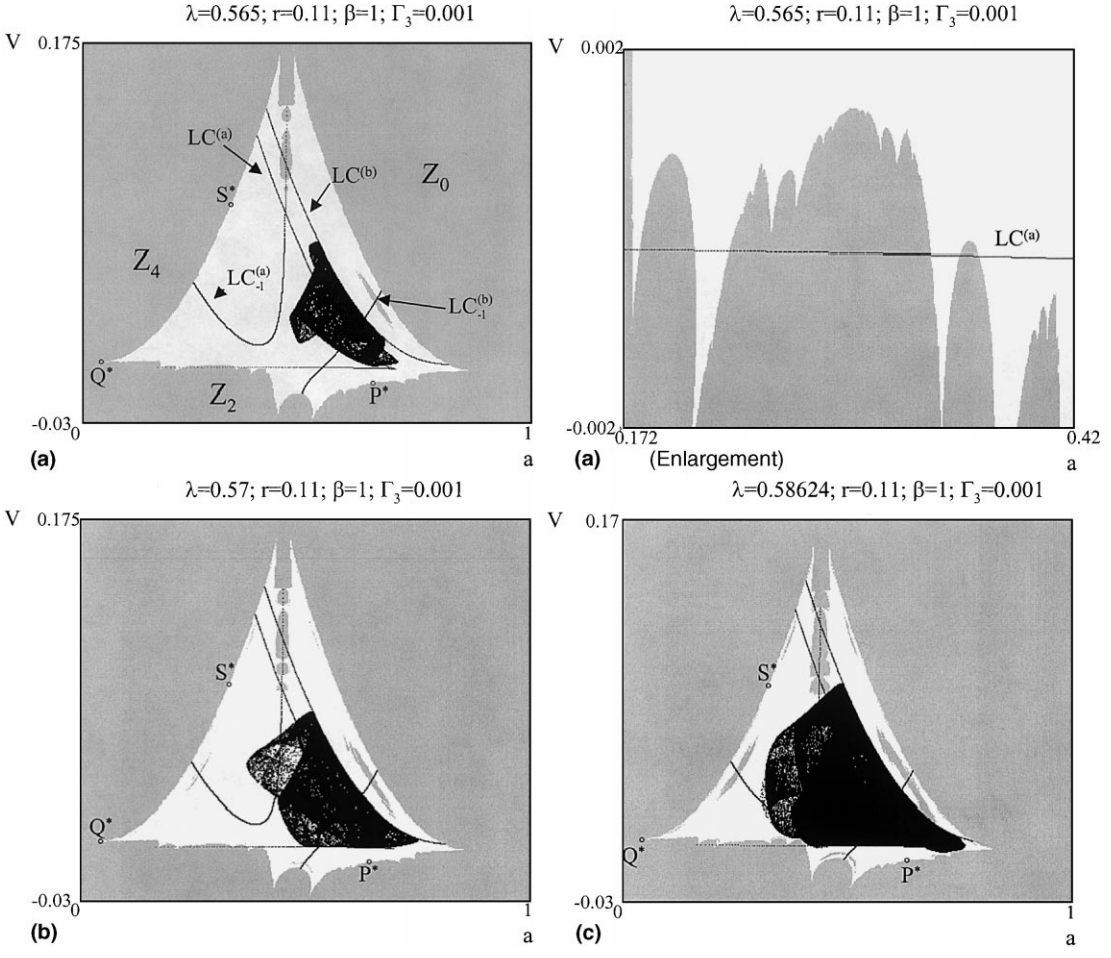

Fig. 7. Chaotic attractors of different shapes in the non- symmetric case with $\beta = 1$. (a) The number of "holes" in the basin of bounded trajectories is now increased. In the enlargement the new contacts of the frontier $\mathscr{F}$ with $LC^{(a)}$ are shown. The chaotic area is bounded by a few segments of critical curves $LC_j^{(b)}$. (b) The chaotic area crosses also $LC_{-1}^{(a)}$ and the boundary of the chaotic area now includes also segments of $LC_j^{(a)}$. Due to the crossing of H_{-1} with the region Z_4 now the grey holes are infinitely many. (c) The chaotic area is now very close to the frontier of its basin.

two-dimensional non-invertible maps, in which the contact between an invariant chaotic area and the boundary of its basin occurs when the invariant area has not completely filled the basin (differently from what was exceptionally found in the example shown in Fig. 4(e)). In this generic case it is very difficult to understand whether some attracting set survives or not. A cycle of high period and very small basin of attraction may exist, not only after the contact, but also in the case shown in Fig. 7(c), although it is numerically not detectable. However, we also note that such cases are of less importance from an applicative point of view, where the generic behaviour is considered as representative of the dynamics of the system.

7. Conclusions

The model of fluctuating growth presented in this paper gives rise to several kinds of dynamic behaviours. Although almost analytically intractable, we have shown how several dynamical properties can be explained by using theoretical arguments coupled with numerical tools. The global bifurcations of the basins of attractions described in Sections 5 and 6 show that local stability is often not enough to consider a model as stable or suitable for the applications. Whereas the arguments in Section 5.2 show that we may have different co-existing attractors whose basins have complex structures, which gives rise to the unpredictability of the asymptotic behaviour for a generic point in the region of interest.

The cases we have considered certainly do not cover all the possible dynamics. However, by applying the techniques which make use of the global basins and of the critical curves, as described in Sections 5 and 6, we hope that other kinds of dynamics can be explained, both locally and globally, as well as new bifurcation mechanisms.

From an applicative point of view we are led to be cautions with our models. Given a situation which defines the parameters' values, we can describe the time evolution and realize if we are in a stable regime or in a regime with oscillatory cycles or in a complex one, and whether particular attention must be paid to small perturbations, which may drastically change the time evolution. We hope that the knowledge of the parameters' regimes, specially those "more critical" for the dynamics, may be of help also to guide the operators.

Acknowledgements

The work has been performed under the activity of the national research project "Dinamiche non-linearied applicazioni alle scienze economiche e sociali", MURST, Italy and under the auspices of CNR, Italy.

Appendix A

In this appendix we consider the map T_0 in (21) and determine its fixed points, solutions of the algebraic system (21) with $\Gamma_3 = 0$, that is

$$\begin{aligned} &-\Gamma_0 + (\Gamma_1 - 1)a - \Gamma_2 a^2 - \Gamma_2 V = 0, \\ &V[\Gamma_2^2(\beta - 1)V + (2\Gamma_2 a - \Gamma_1)^2 - 1] = 0. \end{aligned} \tag{A.1}$$

As observed in Section 5, the a-axis is trapping for the map T_0, and the restriction to this axis is conjugated to the standard logistic map. Thus, assuming $\Delta > 0$, where $\Delta = (\Gamma_1 - 1)^2 - 4\Gamma_0\Gamma_2$, two fixed points are on the a-axis, say Q^* and P^*. The solutions obtained with $V = 0$ in the first equation of (A.1), $a_Q^* = (\Gamma_1 - 1 - \sqrt{\Delta})/2\Gamma_2$ and $a_P^* = (\Gamma_1 - 1 + \sqrt{\Delta})/2\Gamma_2$, give the two fixed points of the map T_0:

$$Q^* = \left(\frac{\Gamma_1 - 1 - \sqrt{\Delta}}{2\Gamma_2}, 0\right) \quad \text{and} \quad P^* = \left(\frac{\Gamma_1 - 1 + \sqrt{\Delta}}{2\Gamma_2}, 0\right). \tag{A.2}$$

Two other fixed points exist.

- For $\beta > 1$, substituting $V = 1 - (2\Gamma_2 a - \Gamma_1)^2)/\Gamma_2^2(\beta - 1)$ in the first equation we get, after rearranging, $\gamma_0 + \gamma_1 a + \gamma_2 a^2 = 0$, where $\gamma_0 = -1 + \Gamma_1^2 - \Gamma_0\Gamma_2(\beta - 1)$, $\gamma_1 = \Gamma_2(\Gamma_1 - 1)(\beta - 1) - 4\Gamma_1\Gamma_2$, $\gamma_2 = \Gamma_2^2(5 - \beta)$, which gives the values $a_S^* = (-\gamma_1 - \sqrt{\gamma_1^2 - 4\gamma_0\gamma_2})/2\gamma_2$ and $a_R^* = (-\gamma_1 + \sqrt{\gamma_1^2 - 4\gamma_0\gamma_2})/2\gamma_2$, thus the two fixed points of the map T_0 are:

$$S^* = \left(a_S^*, V_S^*\right) \quad \text{and} \quad R^* = \left(a_R^*, V_R^*\right), \tag{A.3}$$

where $V^* = (1 - (2\Gamma_2 a^* - \Gamma_1)^2)/(\Gamma_2^2(\beta - 1))$.
- For $\beta = 1$, from the second equation in (A.1) we get $a_S^* = (\Gamma_1 - 1)/2\Gamma_2$ and $a_R^* = (\Gamma_1 + 1)/2\Gamma_2$, and by using the first equation we obtain:

$$S^* = \left(\frac{\Gamma_1 - 1}{2\Gamma_2}, \frac{\Delta}{4\Gamma_2^2}\right) \quad \text{and} \quad R^* = \left(\frac{\Gamma_1 + 1}{2\Gamma_2}, \frac{\Delta - 4}{4\Gamma_2^2}\right). \tag{A.4}$$

The local stability of the fixed points depends on the eigenvalues of the Jacobian matrix of (21) given by

$$J(a, V) = \begin{bmatrix} \Gamma_1 - 2\Gamma_2 a & -\Gamma_2 \\ -4\Gamma_2(\Gamma_1 - 2\Gamma_2 a)V & (\Gamma_1 - 2\Gamma_2 a)^2 + 2\Gamma_2^2(\beta - 1)V \end{bmatrix} \tag{A.5}$$

evaluated at the fixed points. In points belonging to the a-axis the matrix J is upper triangular with eigenvalues given by $\lambda_1 = \Gamma_1 - 2\Gamma_2 a$ and $\lambda_2 = (\lambda_1)^2$. With $a = a_Q^*$ and $a = a_P^*$ we have the eigenvalues associated with the fixed points on the a-axis. Hence Q^* is a repelling node, being $\lambda_1(Q^*) = 1 + \sqrt{\Delta}$ with eigenvectors $r_1(Q^*) = (1, 0)$, along the a-axis, and $\lambda_2 = \left(1 + \sqrt{\Delta}\right)^2$, with eigenvector $r_2(Q^*) = (1, -((\sqrt{\Delta}(1 + \sqrt{\Delta}))/\Gamma_2))$, whereas P^* has eigenvalues given by $\lambda_1(P^*) = 1 - \sqrt{\Delta}$, with eigendirection along the a-axis, and $\lambda_2(P^*) = (1 - \sqrt{\Delta})^2$, with eigenvector $r_2(P^*) = (1, (\sqrt{\Delta}(1 - (\sqrt{\Delta}))/\Gamma_2))$. For $0 < \Delta < 4$, P^* is an attracting node, becoming a repelling node for $\Delta > 4$. The bifurcation occurring at $\Delta = 4$ is of co-dimension two, having both the eigenvalues equal to 1 in absolute value. It is a flip bifurcation along the a-axis, creating a cycle of period 2, attracting node not only for the one-dimensional restriction but also for the whole map T_0, while in the transverse direction the bifurcation is associated with the eigenvalues +1. Below we shall comment it in the case $\beta = 1$.

It is worth noting that for the restriction of the map T_0 to the a-axis, given in (22), we know all the dynamics, being that of the logistic map, and from the structure of the Jacobian matrix, upper triangular on the a-axis, the property stated above regarding the two eigenvalues holds for any cycle.

Regarding the local stability of the other fixed points, we consider only the case with $\beta = 1$ for which we have simpler explicit solutions. Evaluating the Jacobian matrix (A.5) at S^* we have:

$$J(S^*) = \begin{bmatrix} 1 & -\Gamma_2 \\ -\frac{\Delta}{\Gamma_2} & 1 \end{bmatrix}. \tag{A.6}$$

The matrix (A.6) has real eigenvalues for $\Delta > 0$, given by $\lambda_1(S^*) = 1 + \sqrt{\Delta}$ with eigenvector $r_1(S^*) = \left(1, -\sqrt{\Delta}/\Gamma_2\right)$, and $\lambda_2(S^*) = 1 - \sqrt{\Delta}$ with eigenvector $r_2(S^*) = \left(1, \sqrt{\Delta}/\Gamma_2\right)$. Therefore, for $0 < \Delta < 4$, S^* is a saddle point, with local stable manifold tangent to r_2 and the unstable one tangent to r_1, while for $\Delta > 4$ the saddle becomes a repelling node, via flip-bifurcation (the eigenvalue λ_2 crosses through -1), creating a 2-cycle saddle.

For the local stability of R^* we consider the Jacobian matrix

$$J(R^*) = \begin{bmatrix} -1 & -\Gamma_2 \\ \frac{\Delta - 4}{\Gamma_2} & 1 \end{bmatrix}$$

which has real opposite eigenvalues if $\Delta < 5$, being $\lambda_1(R^*) = \sqrt{5-\Delta}$ and $\lambda_2(R^*) = -\sqrt{5-\Delta}$, and complex ones, with real part 0 (i.e. pure imaginary), otherwise. Hence R^* is a repelling node for $\Delta < 4$, an attracting node for $4 < \Delta < 6$, and a repelling focus for $\Delta > 6$.

The bifurcation occurring at $\Delta = 4$ corresponds to a "change of stability", as in fact the fixed points P^* and R^* merge at this bifurcation value. The fixed point R^* from the half-plane $V < 0$ for $\Delta < 4$, and unstable, enters the half-plane $V > 0$ for $\Delta > 4$ becoming an attracting node.

The bifurcation occurring at $\Delta = 6$ is a resonant Hopf bifurcation associated with the two eigenvalues +i and −i (i being the imaginary unit).

Appendix B

In this appendix we consider the rank-1 pre-images of the map T_0 in Eq. (21). Given a generic point of the plane, $p = (a', V')$, then its rank-1 pre-images are the points $(b + (\Gamma_1/2\Gamma_2), V)$ where (b, V) are the real solutions of the algebraic system in (31), which we rewrite for convenience:

$$-\Gamma_2 b^2 - \Gamma_2 V + \frac{\Delta - 1}{4\Gamma_2} = a' - \frac{\Gamma_1}{2\Gamma_2}, \qquad \Gamma_2^2(\beta - 1)V^2 + 4\Gamma_2^2 b^2 V = V'. \tag{B.1}$$

From the first equation of (B.1) we can write

$$b^2 = -V + \frac{\Delta - 1}{4\Gamma_2^2} + \frac{\Gamma_1 - 2\Gamma_2 a'}{2\Gamma_2^2} \tag{B.2}$$

and substituting into the second equation of (B.1) we get a quadratic equation in $V : -V' + \alpha_1 V + \alpha_2 V^2 = 0$, where $\alpha_1 = \Delta - 1 + 2(\Gamma_1 - 2\Gamma_2 a')$ and $\alpha_2 = \Gamma_2^2(\beta - 5)$. It follows that when $\sigma = (\alpha_1^2 + 4\alpha_2 V') < 0$ then the point p has zero rank-1 pre-images. While for $\sigma > 0$ then two values for V exist, given by $V = V_- = (-\alpha_1 - \sqrt{\sigma})/2\alpha_2$ and $V = V_+ = (-\alpha_1 + \sqrt{\sigma})/2\alpha_2$, which are to be substituted in (B.2). Thus two solutions (i.e. two rank-1 pre-images of p) are get if

$$\left(-V_- + \frac{\Delta - 1}{4\Gamma_2^2} + \frac{\Gamma_1 - 2\Gamma_2 a'}{2\Gamma_2^2} \right) > 0$$

and two more pre-images if

$$\left(-V_+ + \frac{\Delta - 1}{4\Gamma_2^2} + \frac{\Gamma_1 - 2\Gamma_2 a'}{2\Gamma_2^2} \right) > 0.$$

References

[1] C. Mira, L. Gardini, A. Barugola, J.C. Cathala, Chaotic Dynamics in Two-Dimensional Non-Invertible Maps, World Scientific, Singapore, 1996.
[2] R. Abraham, L. Gardini, C. Mira, Chaos in Discrete Dynamical Systems (a Visual Introduction in Two-Dimension), Springer, Berlin, 1997.
[3] D. Delli Gatti, M. Gallegati, Financial fragility, fluctuations and growth, beyond the representative agent, mimeo, 1998.
[4] S. Myers, N. Majluf, Corporative financing and investment decisions when firms have informations that investors do not have, J. Financial Econom. 13 (1984) 187–221.
[5] R. Gordon, B. Malkiel, Corporation finance, in: H. Aaron, J. Pechman (Eds.), How Taxes Affect Economic Behaviour, Brooking Institution, Washigton, DC, 1981.

[6] E. Altman, A further empirical investigation of the bankruptcy cost question, J. Finance 39 (1984) 1067–1089.
[7] S. Gilson, Bankruptcy, boards, band and blockholder: evidence on changes in corporate ownership an control when firms default, J. Financial Econom. 27 (1990) 355–388.
[8] S. Kaplan, D. Reishus, Outside directorship and corporate performance, J. Financial Econom. 27 (1990) 389–410.
[9] J.M. Keynes, The General Theory of Employment, Interest and Money, Macmillan, London, 1936.
[10] H. Minsky, John Maynard Keynes, Columbia University Press, New York, 1975.
[11] I. Gumowski, C. Mira, Dynamique Chaotique, Cepadues Editions, Toulose, 1980.
[12] C. Mira, Chaotic Dynamics, World Scientific, Singapore, 1987.
[13] L. Gardini, Homoclinic bifurcations in n-dimensional endomorphisms, due to expanding periodic points, Non-linear Analysis, T.M.A. 23 (1994) 1039–1089.
[14] P. Collet, J.P. Eckmann, Iterated maps on the interval as dynamical systems, Birkhäuser, Boston, 1980.
[15] F.R. Marotto, Snap-back repellers imply chaos in R^n, J. Math. Anal. Appl. 63 (1978) 199–223.
[16] C. Mira, D. Fournier-Prunaret, L. Gardini, H. Kawakami, J.C. Cathala, Basin bifurcations of two-dimensional non-invertible maps: fractalization of basins, Int. J. Bifurcation and Chaos 4 (2) (1994) 343–381.
[17] R.L. Devaney, An Introduction to Chaotic Dynamical Systems, The Benjamin/Cummings, Menlo Park, CA, 1987.